Chemical Geology 384 (2014) 149–167

Contents lists available at ScienceDirect

Chemical Geology

journal homepage: www.elsevier.com/locate/chemgeo

Small-volume baddeleyite (ZrO_2) U–Pb geochronology and Lu–Hf isotope geochemistry by LA-ICP-MS. Techniques and applications

Mauricio Ibanez-Mejia [a,*], George E. Gehrels [a], Joaquin Ruiz [a], Jeffrey D. Vervoort [b], Michael P. Eddy [c], Chen Li [a]

[a] Department of Geosciences, The University of Arizona, Tucson, AZ, USA
[b] School of the Environment, Washington State University, Pullman, WA, USA
[c] Earth, Atmospheric and Planetary Sciences Department, Massachusetts Institute of Technology, Cambridge, MA, USA

ARTICLE INFO

Article history:
Received 17 February 2014
Received in revised form 10 July 2014
Accepted 11 July 2014
Available online 22 July 2014

Editor: K. Mezger

Keywords:
Baddeleyite
U–Pb geochronology
Lu–Hf
LA-ICP-MS
Large igneous provinces

ABSTRACT

U–Pb geochronology of baddeleyite (ZrO_2) is an increasingly used tool in the Earth and planetary sciences for determining the crystallization and emplacement ages of mafic igneous rocks. Additionally, baddeleyite has a strong affinity for hafnium and preferentially excludes the REE's, making it an important repository of Hf isotopic compositions, which can be used to provide constraints on the origin of these rocks. In this contribution we introduce a technique for U–Pb dating and Lu–Hf isotopic analysis of baddeleyite by LA-MC-ICP-MS. A systematic study of crystals with known ages demonstrates that our methodology is capable of producing $^{207}Pb/^{206}Pb$ results that are precise and accurate to within 1% of their TIMS values at a 2-sigma confidence level, while Phanerozoic crystals can generally be dated to within 1.5 to 3.0% accuracy using their $^{206}Pb/^{238}U$ compositions. These results are routinely reproducible with a variety of laser-spot sizes ranging from 30 to 10 μm in diameter and with crater depths as shallow as ~3 μm in depth. This represents a significant improvement in the sampled volume generally used for LA-ICP-MS geochronology and is a critical step for dating small baddeleyite crystals either as mineral separates or identified in situ within thin sections. No orientation-dependent biases on the measured $^{206}Pb/^{238}U$ values were identified from our data, suggesting that LA-ICP-MS dating of Phanerozoic crystals can be routinely performed without the biases previously reported for SIMS instruments. Our data show that initial $^{176}Hf/^{177}Hf$ ratios can be determined with an accuracy as good as 0.5 εHf units by taking the mean of 10 to 30 individual spot analyses acquired with a 40 μm beam-diameter. These U–Pb and Hf results are comparable to what can be routinely achieved for zircon by LA-MC-ICP-MS. In addition to the methodological approach, we report a high-precision U–Pb TIMS age and four solution-MC-ICP-MS Hf isotopic results for new and/or important baddeleyite localities. These new data are used here to assess the adequacy of our fractionation, interference and mass-bias corrections and can be used as a basis for addressing the accuracy of LA-ICP-MS U–Pb and Lu–Hf data for future inter-laboratory calibration efforts.

1. Introduction

Baddeleyite is a monoclinic zirconium oxide mineral that commonly occurs as an accessory phase in silica-undersaturated igneous rocks of terrestrial and extraterrestrial origin (Heaman and Lecheminant, 1993; Heaman, 2009; Niihara, 2011; Moser et al., 2013). In recent years it has received increased attention from both geochronologists and petrologists because it can provide essential age and isotopic information about mafic rocks, a lithologic group where the more widely used mineral in geochronology, zircon ($ZrSiO_4$), is often not present (Scoates and Chamberlain, 1995; Chamberlain et al., 2010). Experimental determinations of trace-element partitioning between baddeleyite and carbonatitic melts performed by Klemme and Meyer (2003) have shown that U is over an order of magnitude more compatible in its crystal structure than Pb, and as a result baddeleyite commonly displays Pb isotopic compositions that are dominantly radiogenic. The importance of baddeleyite as a robust U–Pb geochronometer is supported by decades of work on this mineral prompted by the seminal contribution of Krogh et al. (1987), and is reflected in the publication of a recent special volume on Lithos (vol. 174, 2013) highlighting baddeleyite. In addition to its application of obtaining crystallization ages, the strong compatibility of Hf coupled with low REE contents makes it an ideal mineral for obtaining precise Hf isotopic ratios and fingerprinting initial $^{176}Hf/^{177}Hf$ compositions (Patchett et al., 1981). These geochemical aspects make baddeleyite an important tool for the study of mafic rocks on Earth through time.

For over three decades, and despite the explosion of routine U–Pb geochronology brought about by low-blank thermal ionization mass spectrometry (TIMS) and more recently by secondary ion mass spectrometry (SIMS) and laser ablation-inductively coupled plasma-mass spectrometry (LA-ICP-MS) methods, the use of baddeleyite as a

* Corresponding author.
E-mail address: ibanezm@email.arizona.edu (M. Ibanez-Mejia).

http://dx.doi.org/10.1016/j.chemgeo.2014.07.011
0009-2541/

geochronometer has remained relatively under-represented in the geological literature. Several challenges have made baddeleyite geochronology less straightforward than its felsic counterpart, zircon. First, the generally small size of igneous baddeleyite crystals has made its extraction from rock samples a challenging task. Recent improvements in mineral separation techniques, like those presented by Söderlund and Johansson (2002), have helped to overcome this difficulty. Secondly, a major practical limitation to baddeleyite dating by small-volume in-situ techniques is the orientation-dependent Pb/U fractionation reported by previous workers using secondary-ion mass spectrometers (SHRIMP, Wingate and Compston, 2000; CAMECA-IMS1270, Schmitt et al., 2010). This complexity has imposed practical limits on the accuracy and precision to which young baddeleyites can be dated using their $^{206}Pb/^{238}U$ composition, and for older samples it presents issues for evaluating complexities in U–Pb systematics because the real magnitude of discordance can be largely obscured by unaccounted instrumental fractionations. Recent efforts made by Li et al. (2010) and Schmitt et al. (2010) have shown that this effect in SIMS can be minimized by the use of oxygen-flooding techniques and they report a reduction in the scatter of measured $^{206}Pb/^{238}U$ values down to ~2%. These orientation-dependent instrumental biases or "orientation effects" have also been reported for minerals such as rutile (Taylor et al., 2012), magnetite (Kita et al., 2010; Kozdon et al., 2010), and sphalerite (Kozdon et al., 2010). Examples of this phenomenon however, are exclusive to studies using ion-probe instruments and, to our knowledge, have not been observed for any phase or isotopic system during LA-ICP-MS analyses. If the hypothesized physical mechanism responsible for this crystal-orientation effect — the channeling of primary ions along low-index directions in the crystal lattice (Valley and Kita, 2009) — is the source of the measured $^{206}Pb/^{238}U$ scatter in baddeleyites, then this effect would likely not be observed during laser ablation analyses due to its fundamentally different and strongly energetic sampling mechanism (Horn, 2008). However, as a proof of concept and in order to account for the possible existence of any orientation-effects in LA-ICP-MS analyses, we conducted a simple but systematic experiment designed to test its potential effect.

A commonly observed feature in mafic rocks with complex time-temperature histories is that, upon metamorphism, baddeleyite can easily be recrystallized to poly-crystalline zircon aggregates under a wide range of P–T conditions (Davidson and van Breemen, 1988; Heaman and Lecheminant, 1993; Söderlund et al., 2008). At first glance this could be perceived as an apparent disadvantage, but if the right analytic approach is taken then age information can be retrieved for both events responsible for crystal-growth and recrystallization. Different techniques have been successfully employed to isolate these two components, by dating the baddeleyite cores to determine protolith crystallization ages and by dating the zircon rims to determine the timing of metamorphism These approaches have, thus far, mostly employed ID-TIMS techniques with separation of the phases achieved either by mechanical abrasion (e.g., Davidson and van Breemen, 1988) or selective chemical dissolution (e.g. Rioux et al., 2010). In a more recent study, Beckman et al. (2014) used a combination of TIMS and SIMS analyses of remnant baddeleyite cores enclosed in zircon overgrowths in order to obtain protolith ages from metamorphosed gabbros of the Norwegian Caledonides.

Despite the lack of experimental diffusion data for U or Pb in baddeleyite, the retention of concordant or only slightly discordant U–Pb ages from baddeleyite cores that have undergone granulite-grade metamorphism indicates a high closure temperature for the U–Pb baddeleyite geochronometer (Davidson and van Breemen, 1988; Söderlund et al., 2008; Beckman et al., 2014). Nevertheless, it is well known that the diffusive behavior of any element in a particular mineral phase can be strongly influenced by the structural integrity of the crystal lattice, and therefore radiation-induced damage at the time of reheating may play an important role in the degree of discordance (i.e., age resetting) that a mineral system will attain (Cherniak et al., 1991; Mezger and Krogstad, 1997; Cherniak and Watson, 2000; Geisler et al. 2002). In contrast to zircon, where increased radiation dosage through time leads to amorphisation of the crystalline structure (Murakami et al., 1991), it has been shown that monoclinic zirconia is highly resilient to elevated degrees of radiation dosage and undergoes phase transitions to higher-symmetry polymorphs before experiencing metamictization (Sickafus et al., 1999; Simeone et al., 2002, 2006; Valdez et al., 2008). This process, although not yet fully understood or even observed for natural baddeleyites, may have profound implications for the U–Pb systematics of this mineral because localized phase transformations can lead to the development of diffusion sub-domains and create 'fast-paths' through which Pb could become mobile via grain-boundary diffusion.

The development and improvement of techniques capable of producing texturally-resolved analyses in baddeleyites will not only have an impact on its routine application to dating mafic rocks but will also improve our understanding of its U–Pb systematics in ways that are inaccessible to single- or multiple-crystal-dissolution dating methods. In this contribution, we present an analytical method that allows for the rapid, accurate and spatially resolved dating of baddeleyite using LA-MC-ICP-MS, as well as for investigating their Hf isotopic compositions. We also introduce high-precision ID-TIMS and U–Pb and solution-MC-ICP-MS Hf results for new reference crystals and highlight some of the challenges involved in the accurate and precise estimation of baddeleyite U–Pb crystallization ages. These results are a contribution to the PlasmAge LA-ICP-MS network (www.plasmage.org) and EARTHTIME initiative (www.earth-time.org), and could be used for future inter-laboratory comparison and calibration efforts on baddeleyite geochronology (e.g., Bowring et al., 2013 and Kosler et al., 2013 for zircon).

2. Analytical approach, instrumentation and methods

For this study we used baddeleyite crystals with a wide range of ages that formed in a variety of tectonic settings and host-rock compositions. From oldest to youngest, we present results from the Phalaborwa carbonatite massif of South Africa (2059 Ma, Heaman, 2009; Rioux et al., 2010; Wu et al., 2011), the Tomashgorod dolerite of the Ukrainian Shield (1791 Ma, Bogdanova et al., 2013), the Mackmyra, Sorkka and Ämmänpelto dolerites of Fennoscandia in SE Sweden and SW Finland (1258 to 1256 Ma, Suominen, 1991; Soderlund et al., 2004; 2006), the Duluth Complex FC-1 anorthositic gabbro of Minnesota (1099 Ma, Paces and Miller, 1993), the Gällsjön dyke from the Blekinge–Dalarna swarm in eastern Sweden (956 Ma, Ulf Söderlund, personal communication), the Ogden gabbro from the South Carolina Appalachians (412 Ma, this study), the Kovdor carbonatite massif of the Kola Peninsula in Russia (378 Ma, Amelin and Zaitsev, 2002; Rodionov et al., 2012; Schmitt et al., 2010), and the Yinmawanshan gabbro of the Liaodong Peninsula in China (32 Ma, Li et al., 2010; Yuan et al., 2004; Wu et al., 2006). Most of these baddeleyites have previously been dated by ID-TIMS so they provide a good benchmark for assessing the accuracy and reproducibility of our analytical protocol, while also covering a wide range of geologic time; the only exception is the Yinmawanshan gabbro whose age was estimated by baddeleyite SIMS and zircon LA-ICP-MS methods. Most of them, however, had not been previously studied for their Hf isotopic compositions. In order to address the accuracy and reproducibility of our laser-ablation Lu–Hf results, four key samples were also analyzed by solution-MC-ICP-MS to obtain precise $^{176}Hf/^{177}Hf$ reference ratios.

2.1. LA-MC-ICP-MS uranium–lead geochronology

U–Pb isotopic analyses conducted by LA-MC-ICP-MS were all performed at the Arizona Laserchron Center (ALC) at the University of Arizona (www.laserchron.org). The ALC houses a Photon Machines Analyte-G2 ArF Excimer laser-ablation system using a small-volume,

fast-washout HelEx sample cell. The laser was fired using a repetition rate of 7 Hz, a constant fluency of ~7 J/cm^2 with an energy attenuation of 8%, and a total carrier gas flow of 0.250 SLPM of ultra-high purity He; we found these parameters to produce a stable signal in the mass spectrometer, good sensitivity and a final pit depth that never exceeded a 1:1 width to depth ratio. The laser is coupled to a Nu Instruments HR-MC-ICP-MS with a collector block equipped with 12 Faraday detectors using 3×10^{11} Ω resistors and four discrete dynode ion-counters (Table 1). For 'large' ablation spot sizes (30 μm) the 238, 232, 208, 207 and 206 masses were simultaneously monitored in Faraday collectors while 204 and 202 were measured on ion multipliers. This configuration is referred to as FAR within the text. For small ablation spot sizes (≤15 μm), masses 208, 207, 206 and 204 were all simultaneously monitored on ion-counting detectors in order to allow for higher intensity measurements of the Pb isotopes with low ablation volumes; this latter configuration is referred to as IC within the text.

One of the main challenges involved in working with baddeleyites is the small crystal size found in most rock types, and for this reason we place special effort in obtaining reliable results using the smallest ablation volumes possible. We conducted experiments with spot-sizes ranging from 30 μm to 8 μm in diameter and ablation depths on the range of ca. 8 μm to 3 μm.

2.1.1. Data acquisition and processing

The Nu Plasma ICP-MS offers two different modes of data acquisition: Isotope Analysis (IA) and Time-Resolved Analysis (TRA). Under IA mode, the acquisition routine has the capability of displaying real-time integrated isotopic ratios on the computer screen as the analysis progresses; however, the shortest integration time using this approach is 1 s. In TRA mode, no ratios are calculated in real time during acquisition and results can only be evaluated by processing the raw data after the analysis. The advantage of running in TRA mode is that voltages on each channel can be integrated for much shorter times, allowing for better time-resolved analysis; this becomes necessary for the short-burst routines described below. In this study, we used IA acquisitions for our LA Lu–Hf analysis and U–Pb large-spot (FAR) isotopic analyses, whereas all small-spot (≤15 μm) IC acquisitions were performed on TRA mode using an integration time of 0.2 s.

Data processing was carried out offline using our in-house Excel® VBA macro *bd-agecalc*. Following acquisition, this macro is able to extract data from the raw data files, perform all necessary corrections, and generate a final output table with ages, uncertainties and error correlations by following the procedures described in the following sections (this macro is available from the authors upon request). For analyses conducted using the FAR method, uncertainty propagation and reporting methods followed those discussed by Gehrels et al. (2008), Gehrels et al. (2009) and Cecil et al. (2011) for zircon analyses. For analyses conducted on TRA mode, a slightly modified error propagation and reporting scheme was adopted and will be discussed in Section 2.1.4 when the fractionation-correction strategies are introduced.

2.1.2. Time-dependent fractionation correction

A well-know phenomenon in LA-ICP-MS analysis is the time-dependent elemental fractionation that occurs as a function of increasing pit-depths during the excavation of a single ablation spot (Jackson et al., 1992; Horn et al., 2000; Kosler and Sylvester, 2003). Three main approaches have been proposed by previous authors to correct for this phenomenon. The first is to ablate raster-patterns instead of spots on a polished crystal surface, thus preventing the ablation pit from drilling too deep in any particular location and significantly reducing the down-pit fractionation effect (Kosler and Sylvester, 2003). This method, however, is not a feasible option for very small crystal sizes. The second approach is to account for this effect using an intercept method to retrieve $^{206}Pb/^{238}U$ values by performing a linear regression through the measured ratios (e.g., Sylvester and Ghaderi, 1997; Chang et al., 2006; Gehrels et al., 2008; Thomson et al., 2012). Lastly, the third approach consists of modeling the fractionation behavior of the primary standard using some mathematical fit to the primary standard data (e.g., an exponential relation) and then applying this 'best fit' model to correct for fractionation of the unknowns (Paton et al., 2010). For the baddeleyite results presented here, we found that the Pb/U depth-dependent fractionation can be well fitted with a linear function for ablation times at least as long as 15 s (Fig. 1). Therefore, we adopted the linear-regression intercept approach and performed a least-squares fit through the acquired data in order to calculate the $^{206}Pb/^{238}U$ ratio of each individual spot as the *y* intercept of the regression when *x* (acquisition time) equals 0.6 s after the signal first arrives to the collectors (Fig. 1). This delay in data integration is used in order to allow the laser signal to stabilize, as well as to account for the slightly slower response (i.e., longer time constant) of the Faraday collectors with respect to the ion counters.

The small-volume procedures presented here differ fundamentally from previous work performed by Johnston et al. (2009). Instead of using the 'total counts' approach to calculate ratios and uncertainties for small ablation-volume data using counting statistics, our current instrumentation and methods allow us to perform robust downhole fractionation corrections with spot-sizes down to 10 μm in diameter and ca. 3 μm in depth. This not only provides the ability to date small crystals and sort out small-scale textural complexities, but also retains the ability of retrieving vertically resolved data that can provide insights into elemental and isotopic zonations for each excavated pit. Based on optical interferometry measurements performed using a Wyko NT9800 at the University of Arizona, we determined the excavation rate of the laser to be ca. 0.5 μm/s (~0.07 μm/shot), using a 7 Hz repetition rate and a fluency of ~7 J/cm^2 (with an energy attenuation of 8%). The total pit depth for the 40-bursts routine was of ~2.8 μm (Fig. 2), ~5.0 μm for the 70-burst routine, and ~7.7 μm for the 110-burst routine. When using a 10 μm laser beam diameter, the quoted depths translate into sampled baddeleyite volumes of 2.2×10^2, 3.8×10^2 and 6.0×10^2 μm^3, for the 40-, 70- and 110-bursts routines, respectively.

2.1.3. Strategies for minimizing and correcting for external and internal common-Pb contributions

Common-Pb corrections, including analytical blank, are a fundamental part of accurate U–Pb geochronology on any mineral system (Mattinson, 1987; Gehrels et al., 2008; Frei and Gerdes, 2009; Thomson et al., 2012), but are especially important for young and/or relatively unradiogenic phases. Also, minimizing the external common-Pb (Pbc) contribution is critical for enhancing the isotope-ratio accuracy of short-burst and/or single-shot analyses (Cottle et al., 2009). In order to accomplish this, all our epoxy plugs are thoroughly cleaned before they are loaded inside the laser chamber; this procedure consists of a 5-minute ultrasonic bath with samples immersed in a dilute acid

Table 1
Collector configurations used on the Nu-Plasma for the different modes of acquisition discussed throughout the text.

Type of analysis:	Ex-H	H1	H2	Ax	L1	L2	L3	L4	L5	L6	L7	L8	IC0	IC1	IC2	IC3
U–Pb Faraday mode	238	232								208	207	206	204		202	
U–Pb ion-counter mode	238	232											208	207	206	204
Lu–Hf laser ablation			180	179	178	177	176	175	174	173	172	171				

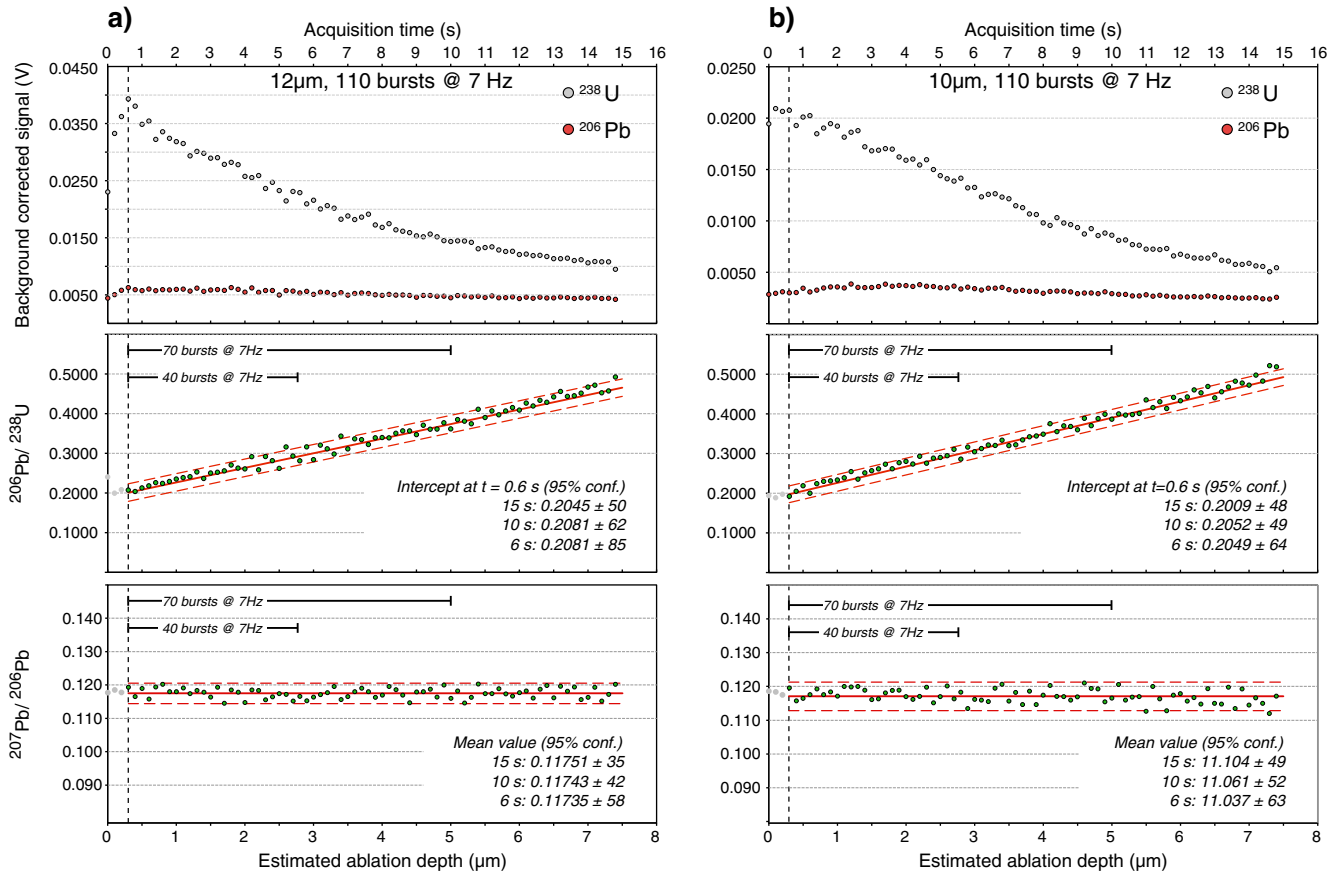

Fig. 1. Examples of measured ^{238}U and ^{206}Pb ion-beam intensities and resulting $^{206}Pb/^{238}U$ and $^{207}Pb/^{206}Pb$ values from ablation of FC-1 baddeleyite. Also shown are their respective down pit-fractionation-corrected $^{206}Pb/^{238}U$ values and average calculations of $^{207}Pb/^{206}Pb$ for 15, 10 and 6 s ablation times. a) 12 µm spot diameter and b) 10 µm spot diameter.

solution (1%HCl–1%HNO_3), followed by soaking in isopropyl alcohol in order to remove all particles and oil coatings that may have resulted from surface polishing and mount handling. When samples are loaded in the laser chamber, the surface of all crystals to be analyzed is cleaned using a 'pre-ablation' routine like that described in Cottle et al. (2012). Our procedure consists of using a larger (~5×) beam diameter than what will be used later for conducting the analysis, and the surface is ablated using three single laser-pulses while carrier gas is flowing through the chamber at a rate of ~1.0 L/m; this material is vented out of the line and is not measured on the mass-spectrometer. The above procedure results in pre-ablation craters that are approximately ~0.12 µm in depth (estimated from optical interferometry), and therefore do not appreciably perturb the observed down-pit fractionation behavior of the analysis. They do, however, significantly improve the accuracy of the measured $^{207}Pb/^{206}Pb$ isotopic compositions obtained with the short-burst routine. Fig. 3 shows an example of two, 15 s ablation passes conducted on a large baddeleyite crystal from the Sorkka dolerite without pre-ablation treatment (Fig. 3a), and after the surface has been pre-ablated (Fig. 3b). It is evident that the pre-ablation routine is effective for reducing surficial common-Pb contamination, which is indicated by spikes in the initial 208, 207 and 204 signals (Fig. 3a). All the small-spot IC data discussed below were acquired using this pre-ablation procedure on both standards and unknowns.

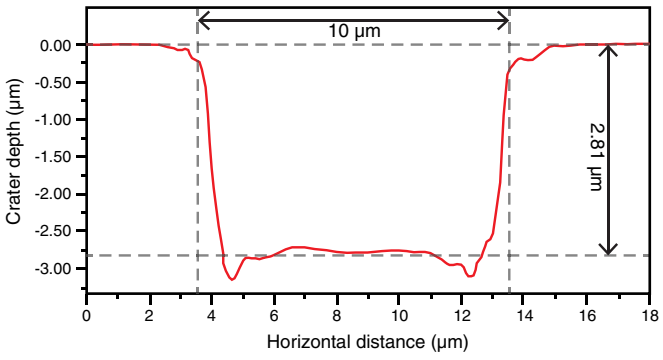

Fig. 2. Cross-sectional profile of an ablation pit in baddeleyite, acquired using a Wyko NT9800 optical interferometer. This crater was produced using 40 laser-bursts firing at a repetition rate of 7 Hz and using a constant fluency of ~7 J/cm^2 with an energy attenuation of 8%. The total crater depth of ca. 2.8 µm indicates a laser excavation rate of ca. 0.5 µm/s or 0.07 µm/shot.

When analyzing samples using the IC collector configuration, monitoring the ^{202}Hg mass was not possible (Table 1). It is worth mentioning, however, that during the majority of our FAR runs there were no detectable increases in the ^{202}Hg signals when the laser was fired (i.e., considered below detection when mean 202 cps of laser-on signal is less than three standard deviations above the background mean value before the laser is fired). Therefore, for our IC sessions, ^{204}Pb ion-beam intensities for each analyzed spot are estimated by performing a $^{204}(Hg + Pb)$ baseline correction to the laser signal, and attributing all of the 204 signal increase to ^{204}Pb. In practice, given the strongly radiogenic compositions observed in all of our analyses (99% of all measured $^{206}Pb/^{204}Pb$ compositions were higher than 1000, and 84% were higher than 5000; see Supplementary material), the impact of not monitoring ^{202}Hg for our Pbc corrections is small to almost negligible. When ^{204}Pb signals were found to be above background, common-Pb corrections were applied using the model of Stacey and Kramers (1975) and additional uncertainties of 1.0% for $^{206}Pb/^{204}Pb$ and 0.3% for $^{207}Pb/^{204}Pb$

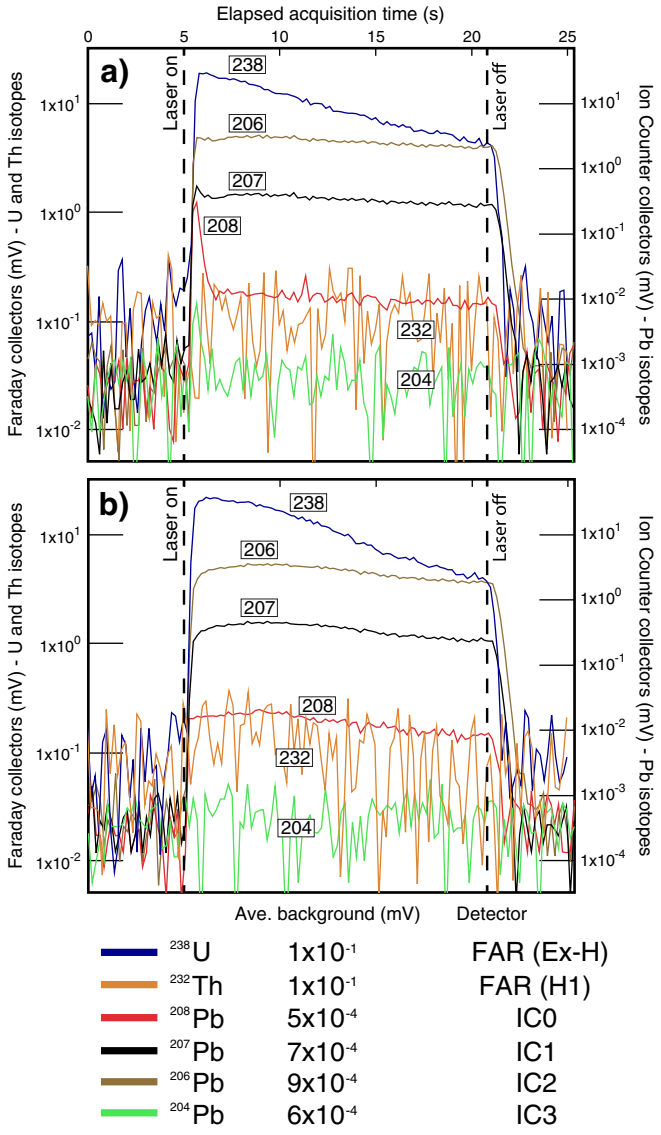

Fig. 3. Comparison of ion intensities generated by ablation of a 1256 Ma baddeleyite crystal from the Sorkka dolerite with a) no pre-ablation treatment and b) data recorded from the same crystal after pre-ablation as described in the text. Notice the conspicuous intensity spikes in the ^{208}Pb, ^{204}Pb, and to a lesser degree ^{207}Pb and ^{206}Pb channels at $t \approx 6$ s when acquiring without pre-ablation cleaning. Both acquisitions made by using 110 bursts of a 10 μm wide laser-beam, firing at a repetition rate of 7 Hz.

were assigned. These uncertainties were propagated throughout the age calculations as described by Gehrels et al. (2008).

2.1.4. Matrix-matched Pb/U fractionation corrections and error propagations

One of the major challenges of accurate U–Pb geochronology by LA-ICP-MS is accounting for the well-known mass and inter-element instrumental fractionations that are induced during the measuring process, and that are identified as an offset in the observed isotopic ratios in samples of known ages. This offset between the 'known' and the measured values represents the cumulative impact of several factors, including differences in element volatility induced by laser ablation, contrasting thermal ionization potentials, and elemental/mass discrimination in the sampled region of the plasma plume. This fractionation effect also exhibits a strongly matrix-dependent behavior, so using a suitable reference standard or fractionation monitor is one of the most critical steps towards accurate U–Pb dating of any particular phase. Previous attempts to date baddeleyite by LA-ICP-MS have utilized zircon crystals or aspirated solutions as reference for correcting the measured ^{206}Pb/^{238}U values (e.g. Horn et al., 2000; Renna et al., 2011; Xie LieWen et al., 2008). This approach has resulted in extremely reversely discordant analyses that are mostly a consequence of inadequate inter-element Pb/U fractionation corrections. To overcome this issue, our approach uses a matrix-matched primary standardization routine to correct for inter-element and mass-bias instrumental fractionations. The anorthositic gabbros of the Duluth complex are well suited for this, as they have been precisely dated by both zircon (Paces and Miller, 1993) and baddeleyite (Crowley and Schmitz, 2009; Hoaglund, 2010; Schmitt et al., 2010) U–Pb geochronology. Samples from the FC-1 and FC-4b localities contain both minerals, and so the U–Pb systematics of baddeleyite and zircon have been well cross-calibrated. It was shown by Hoaglund (2010), however, that some baddeleyite crystals from the FC-4b are concordant within uncertainty but exhibit a slightly older ^{207}Pb/^{206}Pb age (by ~0.41%) with respect to zircons from the same sample, which was interpreted as resulting from initial disequilibrium compositions of the ^{235}U decay chain. Samples from the FC-1 locality have been shown by Crowley and Schmitz (2009) to yield more concordant results. We use crystals from this last locality as primary reference materials in order to correct for fractionation of our LA-MC-ICP-MS measurements. It is worth mentioning that ID-TIMS analyses of the FC-4b locality presented by Schmitt et al. (2010) show only an ~0.25% age difference between the mean ^{206}Pb/^{238}U and ^{207}Pb/^{206}Pb dates, which is smaller in magnitude than the offset observed by Hoaglund (2010) but overlapping with it within analytical uncertainty when the total errors of both studies are considered.

Fig. 4 shows the fractionation behavior of our primary fractionation monitor over a typical, ~2-hour long session of baddeleyite standards and unknowns using the 6 s burst, 10 μm laser diameter, IC configuration. Instrumental drift corrections are conducted by calculating the average value of the six neighboring standards at any given point (sliding window), and applying this average fractionation value to correct for fractionation of each unknown (Gehrels, et al., 2008). After correcting the data for instrumental drift, we found that using the least-squares intercept method discussed above to calculate the ^{206}Pb/^{238}U values and internal uncertainties for each individual spot commonly results in a slight under-estimation of the errors of the primary reference material (i.e., MSWD values for the weighted mean of the FC-1 measurements are greater than unity). As discussed by Horstwood (2008), Cottle et al. (2012), and recently agreed by the PlasmAge community (www.plasmage.org), the minimum uncertainty of any given measurement should incorporate the background subtraction uncertainty, the calculated internal uncertainty for the measurement itself, and the excess variability observed on the primary reference material used for fractionation correction (i.e., FC-1 baddeleyite in our case). For each of the analytical sessions, we derived a normalization uncertainty factor (or over-dispersion factor, OD) that would be required in order to make the MSWD of the reference material mean equal to unity. This excess scatter was then propagated in quadrature with the calculated uncertainty of each data point in order to obtain the minimum uncertainty of each individual measurement. In the case when the calculated MSWD values of the standards are unity or below, no over-dispersion uncertainties were added. Fig. 4 illustrates this procedure; before accounting for the excess scatter, replicate ^{206}Pb/^{238}U measurements performed on FC-1 baddeleyites and their assigned uncertainties result in a MSWD value of 1.17. In this case, an over-dispersion factor of 1.37% was necessary in order to make the MSWD equal to unity, and this factor was also propagated in quadrature to all unknown measurements. The calculated MSWD value for the ^{207}Pb/^{206}Pb mean in this session was 0.86, so no excess scatter factors had to be further added to the unknown data.

From this it follows that the reported uncertainties for the apparent ages of our LA-MC-ICP-MS analyses are quoted at three levels of increasing uncertainty, in the form ±[X][Y][Z] (columns $\pm 2\sigma^{(a)}$, $\pm 2\sigma^{(b)}$ and $\pm 2\sigma^{(c)}$ in the Supplementary material). The first level [X] refers to the

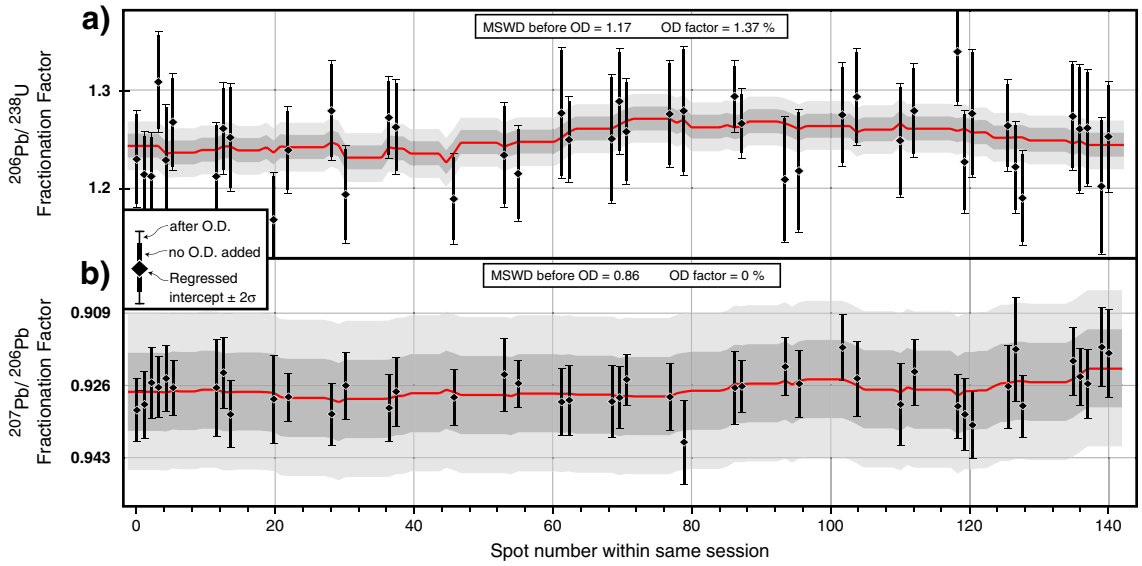

Fig. 4. Example of calculated instrumental fractionation factors for $^{206}Pb/^{238}U$ and $^{207}Pb/^{206}Pb$ ratios using FC-1 baddeleyite crystals as primary reference monitor. Data are from a single session using randomly oriented crystals, where approximately 140 analyses were conducted in a ~2-hour period. Pink line corresponds to the calculated mean of the neighboring six standard measurements. Light-gray shaded area represents the 2% uncertainty range of the measured mean and the dark-gray area is the 1% uncertainty range. Error bars of individual spots are shown at 2σ. See text for details about excess-scatter uncertainty calculations and propagation.

internal uncertainty of each individual analysis derived from the linear-regression to the background-corrected $^{206}Pb/^{238}U$ data, [Y] accounts for the propagation of the excess scatter (or normalization uncertainty) derived for each session, and [Z] is the final total uncertainty that includes the systematic errors associated with the U decay constant, common-Pb corrections and reference-material calibration. Weighted mean ages for cogenetic suites of baddeleyites (igneous samples) reported within the text are quoted with two levels of uncertainty in the form ±(A)[B], where (A) represents the weighted-mean uncertainty calculated using the individual-spot uncertainties [Y] described above (thus incorporating over-dispersion), and [B] represents the total uncertainties after systematic errors have been propagated (accounted for in the uncertainty level [Z]). Discordance is calculated based on the percent discrepancy between the $^{206}Pb/^{238}U$ and $^{207}Pb/^{206}Pb$ mean ages, as Disc. (%) = 100 − (100 ∗ (^{206}Pb / ^{238}U date) / (^{207}Pb / ^{206}Pb date)).

2.2. CA-TIMS uranium–lead geochronology

Five individual baddeleyite crystals from the Ogden gabbro (OG-1) were analyzed by CA-TIMS in the Earth and Planetary Science Department at the Massachusetts Institute of Technology, using the discrete digestion procedures described by Rioux et al. (2010). The annealed crystals were loaded in Teflon microcapsules along with 6.2 N HCl and spiked with EARTHTIME ^{205}Pb–^{233}U–^{235}U (ET535) tracer solution. A single dissolution step for the baddeleyite portion of the grains was achieved by holding the Parr digestion vessel at 210 °C for 60 h. The advantage of the HCl dissolution procedure, in contrast with the more common HF:HNO_3 mix, is that the former has no capacity to dissolve zircon crystals that might be present as inclusions, secondary rims, or as grains adhered to baddeleyite crystals that could go unnoticed during optical inspection. Using this approach, we are confident that the obtained isotopic ratios are representative of the baddeleyites and not a mixture with zircon inclusions or rims that might be present in some samples (Rioux et al., 2010). Following digestion, leachates were run through anion-exchange chromatographic columns to separate U and Pb following the methods of Krogh (1973). Samples were dissolved in H_3PO_4 plus silica-gel and then loaded onto out-gassed zone refined Re filaments. Isotopic analyses were performed on a VG sector 54 thermal ionization mass spectrometer. Fractionation corrections, data reduction and error propagations were done using the U–Pb Redux package (Bowring et al., 2008; McLean et al., 2008). The low common Pb concentrations (≤1 pg Pbc) in each analysis are consistent with its origin as laboratory blank and were subtracted using the MIT Isotope lab Pb blank isotopic composition. Reported ages were corrected for the small ^{206}Pb deficiency that results from the ^{238}U-chain disequilibria generated by low initial Th concentrations.

2.3. Hafnium isotopes by solution-MC-ICP-MS

Baddeleyite crystals from the Duluth complex (FC-1), the Kovdor massif, the Ämmänpelto dolerite (SA-003) and the Ogden gabbro were analyzed by solution MC-ICP-MS in the Radiogenic Isotope and Geochronology Laboratory at Washington State University. The goal of this work was to obtain high-precision $^{176}Hf/^{177}Hf$ values for our reference crystals and to provide a basis for assessing the accuracy of the LA-MC-ICP-MS results. Individual grains or crystal fragments were optically inspected and carefully handpicked under a binocular microscope in order to avoid obvious inclusions or other adhered minerals that could cause contamination. Samples were then loaded in Teflon microcapsules along with 350 μL of 6 N HCl. Sixteen microcapsules were fitted at a time in a large-capacity Parr digestion vessel and heated up to 200 °C for at least 40 h to ensure complete dissolution of the baddeleyite grains.

After complete dissolution was achieved, 20 μL aliquots were taken from each sample for Lu/Hf determinations on a ThermoFinnigan Element2 single collector (SC)-ICP-MS while the remaining 330 μL were processed through ion-exchange liquid chromatography in order to purify the Hf by removing Lu, Yb and the rest of the rare-earth elements. The unspiked, purified Hf solutions were then measured using a ThermoFinnigan Neptune MC-ICP-MS coupled to an Aridus desolvating system. Hf isotope ratios were corrected for mass fractionation using $^{179}Hf/^{177}Hf = 0.7219$ and normalized for instrumental offset using the accepted $^{176}Hf/^{177}Hf = 0.282160$ for the JMC-475 Hf standard solution (Vervoort and Blichert-Toft, 1999). The average measured value for repeated runs of 25 ppb Hf JMC-475 during our analytical session was 0.282136 ± 12 (2 SD, n = 16). These results indicate an external reproducibility of ~0.4 εHf units in the $^{176}Hf/^{177}Hf$

measurements, which was later propagated in quadrature with the in-run errors in order to estimate the total uncertainty for each sample measurement. During the solution analyses, $^{175}Lu/^{177}Hf$ and $^{173}Yb/^{177}Hf$ values were also monitored in order to estimate the degree of residual Lu + Yb interference on mass 176 after ion-exchange purification. Aliquots with total interference corrections ≥0.025% on ^{176}Hf were not included in the calculation of the final weighted-mean values (Table 2), due to significant deviations in $^{176}Hf/^{177}Hf$ compared to results from 'cleaner' aliquots. One exception to this will be discussed below for the Hf results of our Kovdor crystal.

Using the bulk 20 μL aliquots taken before chromatographic purification, $^{176}Lu/^{177}Hf$ compositions were estimated using an Element2 SC-ICP-MS coupled to a spray-chamber sample introduction system at Washington State University. A series of calibration solutions with 1 ppb Hf and different concentrations of Lu ranging from 1 to 0.01 ppb were prepared and measured before and after the unknowns. Sensitivities to ^{175}Lu and ^{173}Yb on the Element2 were on the order of 1×10^6 cps/ppb and signal stability on the calibration solutions was better than 2% RSD for each individual run as well as for the overall calibration factors obtained for the full session.

2.4. Hafnium isotopes by LA-MC-ICP-MS

Laser ablation Lu–Hf isotopic measurements were conducted at the Arizona ALC lab using the same instrumentation as described above for the LA U–Pb analyses. Results presented below were acquired in two separate sessions conducted during October 2012 (Session 1) and January 2013 (Session 2), using ablation spot diameters of 40 μm and 50 μm, respectively. Masses 171 through 180 were all simultaneously monitored on Faraday collectors in order to perform the necessary mass fractionation and isobaric interference corrections (cup configuration shown in Table 1). Mass-bias factors to correct for Hf fractionation (β_{Hf}) were calculated by measuring the $^{179}Hf/^{177}Hf$ value of each analysis and using an exponential fractionation law (Russell et al., 2002) with respect to a reference ratio of 0.7325 (Patchett and Tatsumoto, 1980) as shown in Eq. (1).

$$\beta_{Hf} = \frac{\ln\left(\frac{0.7325}{^{179}Hf/^{177}Hf_{meas}}\right)}{\ln(M179/M177)} \quad (1)$$

Table 2
Solution-MC-ICP-MS Hf isotopic results for reference baddeleyites.

					Interf. after HPLC				
Sample name	Total Hf (V)	$^{176}Hf/^{177}Hf$ (0)[a]	±2σ (in-run)	±2σ (total)[b]	$^{176}Yb/^{177}Hf$[c]	Total int. corr. (%)[d]	$^{176}Lu/^{177}Hf$[e]	$^{176}Hf/^{177}Hf$ (t)	εHf (t)
Duluth gabbro (FC-1) — 1098 Ma									
bd-L-1 (FC-1)	10.9	0.282159	0.000005	0.000013	0.000002	0.001%	0.000122	0.282157	2.4
bd-O-1 (FC-1)	18.3	0.282173	0.000004	0.000013	0.000003	0.001%	0.000077	0.282171	2.9
bd-N-1 (FC-1)	14.5	0.282170	0.000004	0.000013	0.000004	0.002%	0.000092	0.282169	2.8
bd-6-2 (FC-1)	16.1	0.282157	0.000004	0.000013	0.000005	0.002%	0.000076	0.282155	2.3
bd-5-2 (FC-1)	27.2	0.282165	0.000004	0.000013	0.000005	0.002%	0.000108	0.282163	2.6
bd-17-1 (FC-1)	16.6	0.282175	0.000005	0.000013	0.000016	0.006%	0.000157	0.282172	2.9
bd-4-2 (FC-1)	11.4	0.282167	0.000005	0.000013	0.000016	0.006%	0.000099	0.282165	2.7
bd-19-1 (FC-1)[f]	11.6	0.282289	0.000006	0.000014	0.000096	0.043%	0.000144	0.282286	7.0
$^{176}Hf/^{177}Hf_{(0)}$ weighted mean =			0.282167 ± 0.000005 (2σ)		MSWD = 1.09				
Kovdor phoscorite — 378 Ma									
bd-3-2 (Kovdor)	27.3	0.282755	0.000003	0.000013	0.000001	0.000%	0.000009	0.282754	7.3
bd-1-2 (Kovdor)	24.0	0.282758	0.000004	0.000013	0.000002	0.001%	0.000007	0.282758	7.5
bd-22-1 (Kovdor)	11.9	0.282766	0.000005	0.000013	0.000034	0.016%	0.000005	0.282766	7.8
bd-20-1 (Kovdor)	17.9	0.282767	0.000004	0.000013	0.000012	0.006%	0.000004	0.282767	7.8
bd-21-1re (Kovdor)	17.8	0.282773	0.000004	0.000013	0.000028	0.014%	0.000005	0.282773	8.0
bd-23-1 (Kovdor)	22.2	0.282782	0.000004	0.000013	0.000033	0.016%	0.000004	0.282782	8.3
bd-24-1r (Kovdor)[f]	17.2	0.282677	0.000004	0.000013	0.000001	0.001%	0.000007	0.282677	4.6
$^{176}Hf/^{177}Hf_{(0)}$ weighted mean =			0.282767 ± 0.000005 (2σ)		MSWD = 2.44				
Ämmänpelto dolerite — 1256 Ma									
bd-8-2 (SA-003)	15.2	0.282161	0.000005	0.000013	0.000003	0.001%	0.000638	0.282146	5.6
bd-10-2 (SA-003)	27.1	0.282168	0.000003	0.000013	0.000004	0.002%	0.000773	0.282149	5.7
bd-9-2 (SA-003)	25.6	0.282164	0.000003	0.000013	0.000005	0.002%	0.000529	0.282152	5.8
bd-11-2 (SA-003)	25.5	0.282168	0.000003	0.000013	0.000006	0.002%	0.000757	0.282150	5.8
bd-H-1 (SA-003)	19.1	0.282170	0.000003	0.000013	0.000019	0.009%	0.000519	0.282158	6.0
bd-7-2 (SA-003)	22.5	0.282172	0.000003	0.000013	0.000027	0.011%	0.000676	0.282156	6.0
bd-G-1 (SA-003)[f]	11.0	0.282225	0.000005	0.000013	0.000059	0.028%	0.000968	0.282202	7.6
bd-K-1 (SA-003)[f]	10.5	0.282317	0.000006	0.000014	0.000080	0.039%	0.000539	0.282304	11.2
$^{176}Hf/^{177}Hf_{(0)}$ weighted mean =			0.282167 ± 0.000005 (2σ)		MSWD = 0.37				
Ogden gabbro (OG-1) — 412 Ma									
bd-16-2 (Ogden)	5.5	0.282692	0.000008	0.000015	0.000003	0.001%	0.000055	0.282692	5.9
bd-12-2 (Ogden)	5.9	0.282687	0.000008	0.000015	0.000009	0.004%	0.000082	0.282686	5.7
bd-13-2 (Ogden)	6.7	0.282694	0.000006	0.000014	0.000018	0.006%	0.000087	0.282693	5.9
bd-14-2 (Ogden)	3.6	0.282705	0.000010	0.000016	0.000098	0.037%	0.000062	0.282705	6.3
bd-15-2 (Ogden)[f]	1.5	0.282769	0.000019	0.000022	0.000152	0.059%	0.000065	0.282769	8.6
bd-D-1 (Ogden)[f]	2.2	0.282942	0.000015	0.000020	0.000317	0.143%	0.000061	0.282942	14.7
bd-E-1 (Ogden)[f]	4.3	0.282989	0.000009	0.000015	0.000332	0.152%	0.000060	0.282988	16.4
$^{176}Hf/^{177}Hf_{(0)}$ weighted mean =			0.282694 ± 0.000007 (2σ)		MSWD = 0.96				

[a] Normalized with respect to JMC-475: no. of measurements = 16, mean = 0.282136 ± 12 (2σ), Hf bias factor = 1.000084.
[b] Total uncertainties estimated by cuadratically propagating the in-run uncertainties and the external reproducibility of our JMC-475 standard (2 SD = 0.000012).
[c] Calculated ^{176}Yb interferences based on the measured $^{173}Yb/^{176}Hf$ ratios and using the $^{176}Yb/^{173}Yb$ values of Vervoort et al. (2004) as described in the text.
[d] Total interferences are estimated based on the calculated ^{176}Yb and ^{176}Lu (not shown) contributions.
[e] Estimated $^{176}Lu/^{177}Hf$ ratios from Solution-SC-ICP-MS measurements used for radiogenic contribution corrections as described in text.
[f] Analyses not used towards final weighted mean calculations due to elevated Yb interference ratios.

Unlike solution analyses, where the isobaric interferences of ^{176}(Lu + Yb) on ^{176}Hf can be minimized or removed by ion-exchange chromatography, the nature of LA analyses implies that those interferences will be present and have to be appropriately accounted for to obtain accurate ^{176}Hf/^{177}Hf values (Fisher et al., 2014a and references therein). In the presence of a measurable Yb signal, its mass fractionation factor, β_{Yb}, can be calculated using a similar approach to that of Eq. (1) by monitoring two non-interfered masses of Yb (e.g. ^{171}Yb and ^{173}Yb) and comparing it with respect to a reference ratio (Woodhead et al., 2004). For our LA Hf results we applied the Yb model of Vervoort et al. (2004) and calculated β_{Yb} factors by normalizing the measured ^{173}Yb/^{171}Yb with respect to a reference value of 1.129197. Alternatively, in samples where the Yb signal intensities are low—as is the case in many natural baddeleyites—the uncertainties on the calculated β_{Yb} factors can be large due to low count-rates in the Faraday detectors; this would have a negative impact on the accuracy of the estimated ^{176}Yb interferences. To circumvent this issue, an alternative approach consists of approximating the mass-fractionation of Yb from that of Hf. This can be achieved by establishing a robust β_{Hf}–β_{Yb} relation for each particular session, and then apply a modified Hf fractionation value ($x\beta_{Hf}$) to correct for Yb fractionation instead of the measured β_{Yb} when the latter has poor accuracy. This β_{Hf}–β_{Yb} relation should ideally be estimated from the LA-MC-ICP-MS data itself, as potential mass-fractionation differences in the plasma might arise by the use of different sample-introduction systems (Fisher et al., 2014a). In the past, other authors have approached these corrections by measuring a series of Yb-doped JMC-475 solutions to retrieve the mass-fractionation parameters that correct the measured ratios to their known ^{176}Hf/^{177}Hf values (Thirlwall and Walder, 1995; Griffin et al., 2000). However, as illustrated in Fig. 5, this would not be a satisfactory approach to correct for our laser data as utilizing the bias factors derived from the solution measurements would result in significant under-correction for ^{176}Yb interference. In order to perform accurate corrections to the LA results, our reduction routine uses the high-Yb baddeleyite analyses to determine an average, laser-derived and session-specific β_{Hf}–β_{Yb} correlation. This relationship is then used to recast the β_{Hf} of each analysis into a term $x\beta_{Hf}$, which can be used in exchange of the measured β_{Yb} values when correcting the moderate- to low-REE baddeleyites for Yb interference.

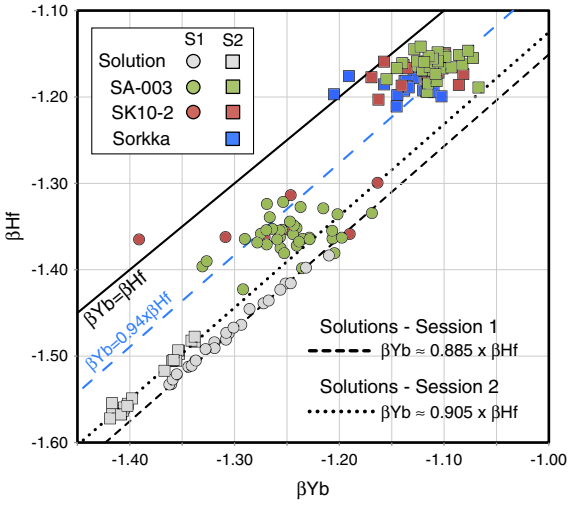

Fig. 5. β_{Hf} vs. β_{Yb} relationships measured for Yb-doped JMC-475 solutions analyzed using a Nu Instruments DSN-100 desolvation nebulizer system (light gray symbols), and by laser-ablation analyses of Ämmänpelto (SA-003 — green), Yinmawanshan (SK10-2 — red) and Sorkka (blue) baddeleyites using the methods described in the text. Note the clustering of the β_{Hf}–β_{Yb} fractionation pairs for each LA session and the consistent departure from the measured solutions values. By using an empirically derived $\beta_{Yb} = x\beta_{Hf}$ relationship, the solution β_{Yb} values are best approximated by an x factor between 0.87 and 0.90 whereas the LA data is in the range 0.91–0.97.

The results obtained by both reduction procedures (i.e., using the measured β_{Yb} and calculated $x\beta_{Hf}$) are presented in the data repository for samples yielding total Yb signals lower than 0.1 V on average.

After the Yb interference correction has been applied, we noticed a small residual negative trend in ^{176}Hf/^{177}Hf vs. ^{176}Yb/^{177}Hf for repeated analyses of cogenetic REE-rich baddeleyites. This indicates a slight overcorrection for ^{176}Yb contributions to the 176 mass, a phenomenon that has also been noted for solution-MC-ICP-MS analyses (Vervoort et al., 2004) and LA-MC-ICP-MS analyses of zircon (Fisher et al., 2011). To compensate for this issue, we derive an empirical secondary Yb correction factor by using our natural reference crystals. Baddeleyites from the Ämmänpelto dolerite (SA-003) have fairly high Yb concentrations, reaching up to 28% in the calculated ^{176}Yb/^{176}(Hf + Yb) interference (see Supplementary material). Assuming that all SA-003 crystals should yield the same ^{176}Hf/^{177}Hf value irrespective of their Yb concentration, which is likely to be the case given their low Lu contents, a bias factor to the reference ^{176}Yb/^{173}Yb composition can be determined such that this slope is minimized (in a way analogous to the secondary Yb correction of Vervoort et al., 2004). This factor was found to average 0.9889 for Session 1 and 0.9909 for Session 2, indicating that a ~1.0 to 1.2% correction to the ^{176}Yb/^{173}Yb reference value was necessary in order to appropriately correct our laser data for ^{176}Yb interference.

Our final mass-bias and interference-corrected ^{176}Hf/^{177}Hf ratios are thus calculated using the following expressions:

$$\frac{^{176}\mathrm{Hf}}{^{177}\mathrm{Hf}_{corr}} = \left[\left(\frac{^{176}(\mathrm{Hf}+\mathrm{Yb}+\mathrm{Lu})_{meas} - ^{176}\mathrm{Yb}_{calc} - ^{176}\mathrm{Lu}_{calc}}{^{177}\mathrm{Hf}_{meas}}\right)\cdot\left(\frac{M176}{M177}\right)^{\beta_{Hf}}\right]\cdot \mathrm{BF}_{Hf} \quad (2)$$

$$^{176}\mathrm{Yb}_{calc} = ^{173}\mathrm{Yb}_{meas}\cdot\left[\frac{^{176}\mathrm{Yb}}{^{173}\mathrm{Yb}_{ref}}\cdot \mathrm{BF}_{Yb}/\left(\frac{M176}{M173}\right)^{(\beta_{Yb})\mathrm{or}(x\beta_{Hf})}\right] \quad (3)$$

$$^{176}\mathrm{Lu}_{calc} = ^{175}\mathrm{Lu}_{meas}\cdot\left[\frac{^{176}\mathrm{Lu}}{^{175}\mathrm{Lu}_{ref}}/\left(\frac{M176}{M175}\right)^{\beta_{Yb}}\right] \quad (4)$$

where M176/M177, M176/M173 and M176/M175 are the ratios of the exact masses of these isotopes of Hf, Yb, and Lu, respectively. The BF_{Yb} term is the secondary Yb correction factor derived from the high-REE baddeleyite measurements, and BF_{Hf} is the instrumental-bias factor for Hf. This last term can be derived from repeated measurements of the JMC-475 solution (Kemp et al., 2009; Cecil et al., 2011), or by normalization with respect to a well-characterized, matrix-matched LA-MC-ICP-MS reference material measured during the same analytical session. Given the current lack of well-characterized, low-REE baddeleyite reference crystals to calculate this bias directly from laser-ablation data, in this contribution we used the value obtained from the measurement of JMC-475 solutions. However, it is expected that this approach may change in the future as suitable reference crystals are calibrated and made available to the community (e.g., mud tank in the case of zircon analyses as advocated by Fisher et al., 2014a).

Repeated measurements of 25 ppb Hf JMC-475 standard solutions performed during Session 1 resulted in an average uncorrected ^{176}Hf/^{177}Hf value of 0.282149 ± 22 (2 SD, n = 6), and those from Session 2 had an average value of 0.282154 ± 13 (2 SD, n = 10). This indicates an average external precision of ca. 0.8 and 0.5 εHf units for the two LA sessions, respectively.

2.5. EBSD crystal-orientation measurements

Large single crystals or crystal fragments of FC-1, Kovdor, Phalaborwa, SA-003 and SK10-2 were randomly oriented in epoxy plugs and the surface of the mount was polished to a high quality, finishing with a chemical polish step in order to remove the strained

layer left after the first phases of mechanical abrasion. Baddeleyites were imaged for cathodoluminescence (CL) using a Gatan Chroma-CL detector and electron back-scattered diffraction patterns were acquired with an Oxford AZtec EBSD system, both of which are attached to a Hitachi 3400 N SEM at the University of Arizona (www.geoarizonasem.org). The obtained Kikuchi diagrams were indexed using the Oxford CHANNEL 5 software (Fig. 6) and orientations were calculated based on the baddeleyite crystal structure (ZrO_2 end member) described by Hann et al. (1985). The difference in orientation resulting from the use of the monoclinic ZrO_2 end-member versus the HfO_2 end-member as reference crystal structures to index our Kikuchi bands resulted in Euler angle mismatches of <2°. Therefore, we are confident that our calculated orientations are accurate independent of the HfO_2 content of the analyzed baddeleyites. Pole figures were calculated and plotted using the MTEX Matlab® toolbox of Bachmann et al. (2010).

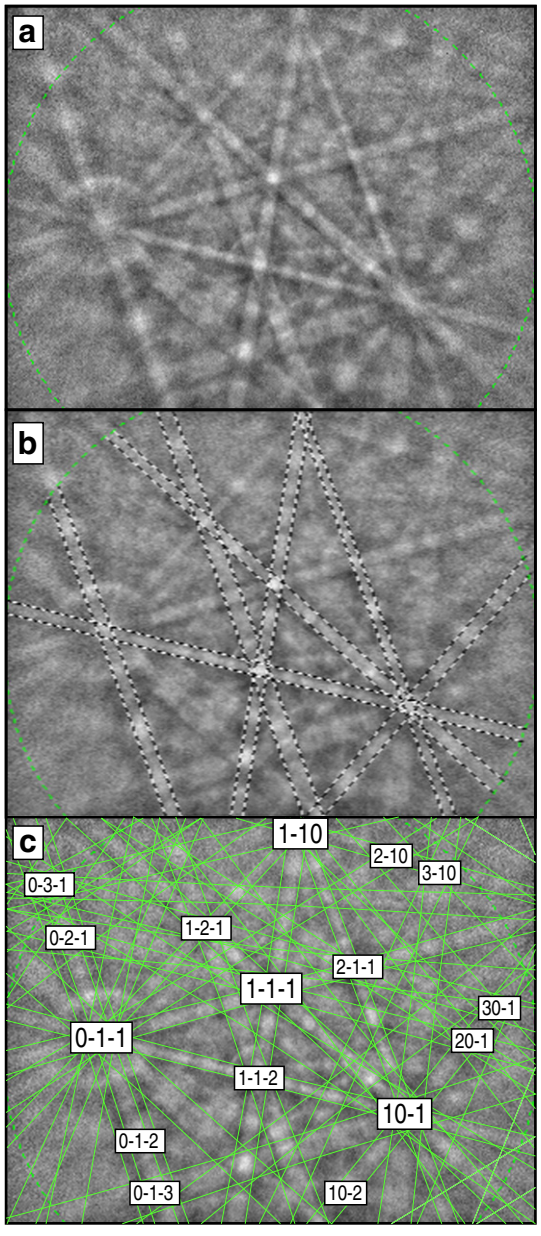

Fig. 6. Example of the fitting procedure followed for indexing EBSD figures and calculating crystallographic orientations: a) raw diffractogram recorded in the phosphorous screen of the Aztec EBSD system from a Kovdor baddeleyite crystal, b) identification of the seven more prominent Kikuchi bands performed by the Oxford CHANNEL5 data processing software, and c) indexing of the Kikuchi bands by using the monoclinic ZrO_2 structure of Hann et al. (1985).

3. Evaluating the crystal-orientation effects on Pb/U fractionation

It was noted initially by Wingate and Compston (2000) during SHRIMP analyses of baddeleyite that, in contrast to zircon and monazite, the former exhibits an excess scatter in the measured $^{206}Pb/^{238}U$ ratios that is reasonably well correlated with the crystallographic orientation of the analyzed surface relative to the incident primary ion beam, and to the local density of twinning planes. This effect has been reported for several different phases analyzed by SIMS (Kita et al., 2010; Kozdon et al., 2010; Taylor et al., 2012) but has never been reported for LA-ICP-MS analyses. One potential complication for assessing orientation-dependent variations in instrumental fractionation of Pb/U values arises from the difficulty of separating this effect from real disturbances in the isotopic system that cause primary or secondary discordance in natural samples (e.g., initial U-series disequilibria, Pb or U mobility, etc.). Since there is little laser-induced fractionation of the $^{207}Pb/^{206}Pb$ ratios during LA-ICP-MS analysis, variable Pb/U instrumental fractionation in concordia space would be represented as an array of ellipses with variable $^{206}Pb/^{238}U$ and $^{207}Pb/^{235}U$ compositions aligned along a common $^{207}Pb/^{206}Pb$ chord. This topology is very similar to what would be expected from samples that have undergone any degree of recent Pb-mobility (loss or gain) and could therefore make the added contribution of these two factors difficult to deconvolve.

Our approach to evaluate this potential orientation-dependent fractionation effect consisted of the following steps: 1) randomly mounted crystal fragments were measured for their crystallographic orientation by EBSD during a single SEM session and were all indexed using the same evaluation parameters; 2) crystals from which good EBSD data were obtained (mean angular deviations <1°) were analyzed by LA-ICP-MS in a random fashion, using the FAR method described above and also within a single analytical session; 3) total age fractionation values were calculated for each individual spot based on the 'known' age of each crystal; 4) a mean fractionation value was calculated from all the obtained data and deviations (in %) from this mean were computed for each one of the individual spots; and 5) these spot deviation values were paired with their EBSD orientation measurements and all results were plotted together as inverse pole-figures for a monoclinic cell (Fig. 7). If an orientation-dependent effect were of significance in the measured fractionations factors, then one would expect clusters of similar percent age deviation to be grouped by regions in the pole figures. However, what is observed in Fig. 7 is a random distribution of both higher- and lower-than-mean values in all regions of the pole figure irrespective of their orientation. These results suggest that orientation-dependent fractionation does not play an important role in the total instrumental fractionation observed in LA-ICP-MS data. Although our observations do not absolutely rule out a potential small contribution of this effect to the total observed fractionation, from our current dataset we conclude that this effect, if present, is indistinguishable within uncertainty from all other sources of scatter that are associated with our measurements. This conclusion is also supported by the general good concordance of our results as will be shown in the next section and the calculated MSWD values close to unity for the $^{206}Pb/^{238}U$ weighted-mean ages obtained on Phanerozoic crystals.

4. Precision, accuracy and reproducibility of LA-MC-ICP-MS U–Pb geochronological results

In an effort to estimate the overall precision, accuracy and reproducibility that can be attained with our analytical methods, we conducted multiple analytical sessions over the last two years focused on measuring the ages of baddeleyite crystals with known isotopic compositions. Experiments were also performed using a variety of spot sizes and crater depths, in order to evaluate the accuracy of the obtained data as

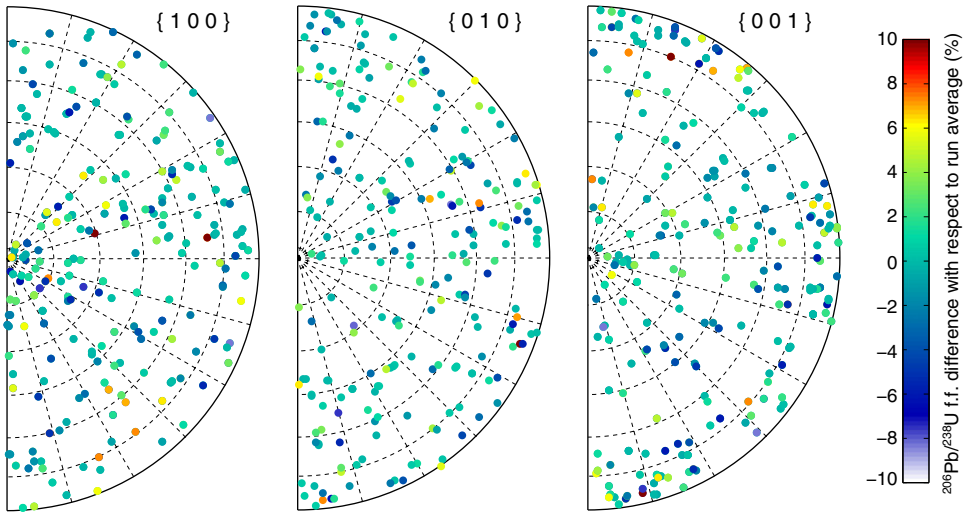

Fig. 7. Deviation from average $^{206}Pb/^{238}U$ fractionation factors as a function of crystallographic orientation relative to the incident laser beam. Plotted values are calculated as the percent difference in individual measured $^{206}Pb/^{238}U$ fractionation with respect to the session-average fractionation (see text for details). Chart was compiled by combining datasets obtained from SA-003, Kovdor, Phalaborwa, FC-1 and SK10-2 crystals. Complete dataset is available from the authors upon request.

we optimize the sampled volume by ablating progressively smaller craters. Fig. 8 shows a few representative concordia diagrams from our dataset, one for each of the samples that was analyzed during the course of this study. These data are taken from different analytical sessions and show the level of precision and accuracy that can consistently be achieved using our routine low-volume approach (i.e., ~9×10^2 μm^3). For Precambrian baddeleyites, in which normal discordance is a commonly observed feature (Soderlund et al., 2013), individual spots that are 5% or more normally discordant were not used towards the $^{206}Pb/^{238}U$ weighted-mean age calculations due to the likelihood of these having experienced some degree of Pb-loss (dashed blue ellipses in Fig. 8). Calculated $^{207}Pb/^{206}Pb$ weighted-mean ages incorporate all analyses shown in the concordia diagrams irrespective of their degree of discordance. The results of all analyses performed during eight different analytical sessions from October 2011 to January 2013 are summarized in Fig. 8. For the interested reader, a similar figure showing the offset of both the $^{207}Pb/^{206}Pb$ and $^{206}Pb/^{238}U$ ages is available as Supplementary material.

Analyses of Paleoproterozoic crystals from the Phalaborwa carbonatitic complex and the Tomashgorod dolerite are all within 0.5% (using measured $^{207}Pb/^{206}Pb$ values) of their published TIMS results and have $^{206}Pb/^{238}U$ weighted-mean ages that are concordant within 2%. Crystals from the Meso- and Neoproterozoic Fennoscandian dolerites show a slightly larger variability but all have $^{207}Pb/^{206}Pb$ ages that are within 0.7% age discrepancy. Results from the Kovdor phoscorites and the Yinmawanshan gabbro display different magnitudes of $^{206}Pb/^{238}U$ age offset and uncertainty that correlate with the acquisition parameters used for each particular session. In general, we note that analyses acquired using the FAR approach have larger uncertainties than those collected with IC due to the low Pb ion-beams in the Faraday collectors, even when a spot size of 30 μm is used. There is a general improvement in the age precision and accuracy using the IC approach. Using this configuration, the age of Kovdor can be reproduced within 1% and with average precision of 2% (2σ confidence). The Yinmawanshan gabbro has not been previously dated by TIMS methods, so addressing the accuracy of our ages is not straightforward. The two available age estimates for this sample are of 32.1 ± 0.5 Ma and 32.9 ± 0.5 Ma, and were obtained by LA-ICP-MS dating of zircons (Yuan et al., 2004) and SIMS dating of baddeleyites (Li et al., 2010), respectively. Most of our calculated ages are clustered around the zircon LA-ICP-MS result, and therefore this is the reference value we used to calculate the discrepancies in the offset chart (Fig. 9). The largest departures from the zircon reference age are of ±3% in magnitude (i.e., ±1 Ma), but still overlap with it within uncertainty. Therefore, we can confidently say that even for crystals as young as Oligocene in age, we are able to routinely retrieve ages that are accurate and precise to within 3%. Nevertheless, note that all age estimates using the 10 μm spot and shortest (6 s) routine are within 2% of age discrepancy.

5. Evidence for intra-crystalline mobility of radiogenic Pb in baddeleyite

The $^{206}Pb/^{238}U$ uncertainties associated with our age calculations are in large part controlled by the primary standardization process (OD factors) and the systematic errors, which together constitute an important part of the quoted total age uncertainties (Figs. 8 and 9). It can be argued that the excess scatter in the $^{206}Pb/^{238}U$ fractionation factors observed from our primary reference material (FC-1 baddeleyite), might in part be controlled by real perturbations to the U–Pb systematics and is not just an artifact of overestimated analytical precision. For all of our runs, we have found a good correlation between the departure-from-average fractionation coefficient of a particular FC-1 analysis and its magnitude of internal U zoning as evidenced by the measured 238 ion-currents. Sharp initial U heterogeneities in these crystals have resulted in complex $^{206}Pb/^{238}U$ zoning profiles within single grains, observed as higher $^{206}Pb/^{238}U$ ratios in low-U zones when adjacent to high-U zones that display variable degrees of Pb-loss (Fig. 10). We interpret this as the result of diffusion-induced radiogenic Pb (Pb*) implantation from high-U zones to low-U zones of the crystal; in a zoned baddeleyite with very low to negligible initial lead (as evidenced by low ^{204}Pb counts), elemental Pb concentration gradients will develop

Fig. 8. Representative U–Pb concordia diagrams for each of the baddeleyite localities analyzed by LA-ICP-MS during the course of this study. All the examples show data acquired using a 10 μm beam and a 6 s ablation duration routine (i.e., ~3 μm in depth). Blue dashed ellipses are >5% normal discordant spots that were not used towards the weighted-mean $^{206}Pb/^{238}U$ age calculations. Red solid ellipses are <5% discordant spots. Uncertainties are quoted to 95% confidence and are shown in the form ± (A)[B] as described in Section 2.1.4. TIMS reference ages quoted for each locality are cited in the text. No $^{207}Pb/^{206}Pb$ ages or concordance values are calculated for Phanerozoic crystals.

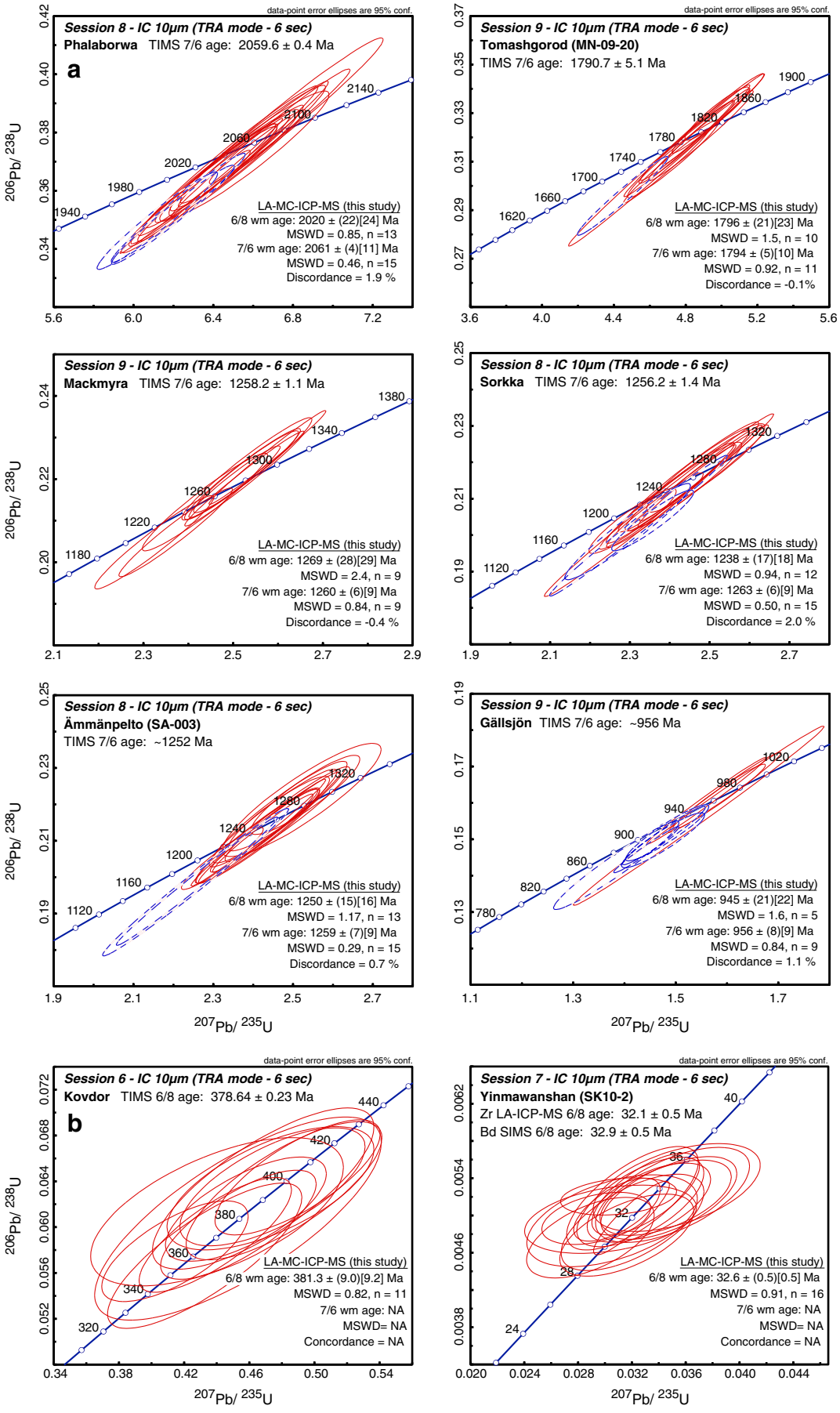
data-point error ellipses are 95% conf.
Session 8 - IC 10μm (TRA mode - 6 sec)
Phalaborwa TIMS 7/6 age: 2059.6 ± 0.4 Ma
a
LA-MC-ICP-MS (this study)
6/8 wm age: 2020 ± (22)[24] Ma
MSWD = 0.85, n =13
7/6 wm age: 2061 ± (4)[11] Ma
MSWD = 0.46, n =15
Discordance = 1.9 %
Session 9 - IC 10μm (TRA mode - 6 sec)
Tomashgorod (MN-09-20)
TIMS 7/6 age: 1790.7 ± 5.1 Ma
LA-MC-ICP-MS (this study)
6/8 wm age: 1796 ± (21)[23] Ma
MSWD = 1.5, n = 10
7/6 wm age: 1794 ± (5)[10] Ma
MSWD = 0.92, n = 11
Discordance = -0.1%
Session 9 - IC 10μm (TRA mode - 6 sec)
Mackmyra TIMS 7/6 age: 1258.2 ± 1.1 Ma
LA-MC-ICP-MS (this study)
6/8 wm age: 1269 ± (28)[29] Ma
MSWD = 2.4, n = 9
7/6 wm age: 1260 ± (6)[9] Ma
MSWD = 0.84, n = 9
Discordance = -0.4 %
Session 8 - IC 10μm (TRA mode - 6 sec)
Sorkka TIMS 7/6 age: 1256.2 ± 1.4 Ma
LA-MC-ICP-MS (this study)
6/8 wm age: 1238 ± (17)[18] Ma
MSWD = 0.94, n = 12
7/6 wm age: 1263 ± (6)[9] Ma
MSWD = 0.50, n = 15
Discordance = 2.0 %
Session 8 - IC 10μm (TRA mode - 6 sec)
Ämmänpelto (SA-003)
TIMS 7/6 age: ~1252 Ma
LA-MC-ICP-MS (this study)
6/8 wm age: 1250 ± (15)[16] Ma
MSWD = 1.17, n = 13
7/6 wm age: 1259 ± (7)[9] Ma
MSWD = 0.29, n = 15
Discordance = 0.7 %
Session 9 - IC 10μm (TRA mode - 6 sec)
Gällsjön TIMS 7/6 age: ~956 Ma
LA-MC-ICP-MS (this study)
6/8 wm age: 945 ± (21)[22] Ma
MSWD = 1.6, n = 5
7/6 wm age: 956 ± (8)[9] Ma
MSWD = 0.84, n = 9
Discordance = 1.1 %
data-point error ellipses are 95% conf.
Session 6 - IC 10μm (TRA mode - 6 sec)
Kovdor TIMS 6/8 age: 378.64 ± 0.23 Ma
b
LA-MC-ICP-MS (this study)
6/8 wm age: 381.3 ± (9.0)[9.2] Ma
MSWD = 0.82, n = 11
7/6 wm age: NA
MSWD= NA
Concordance = NA
data-point error ellipses are 95% conf.
Session 7 - IC 10μm (TRA mode - 6 sec)
Yinmawanshan (SK10-2)
Zr LA-ICP-MS 6/8 age: 32.1 ± 0.5 Ma
Bd SIMS 6/8 age: 32.9 ± 0.5 Ma
LA-MC-ICP-MS (this study)
6/8 wm age: 32.6 ± (0.5)[0.5] Ma
MSWD = 0.91, n = 16
7/6 wm age: NA
MSWD= NA
Concordance = NA
206Pb/ 238U
207Pb/ 235U

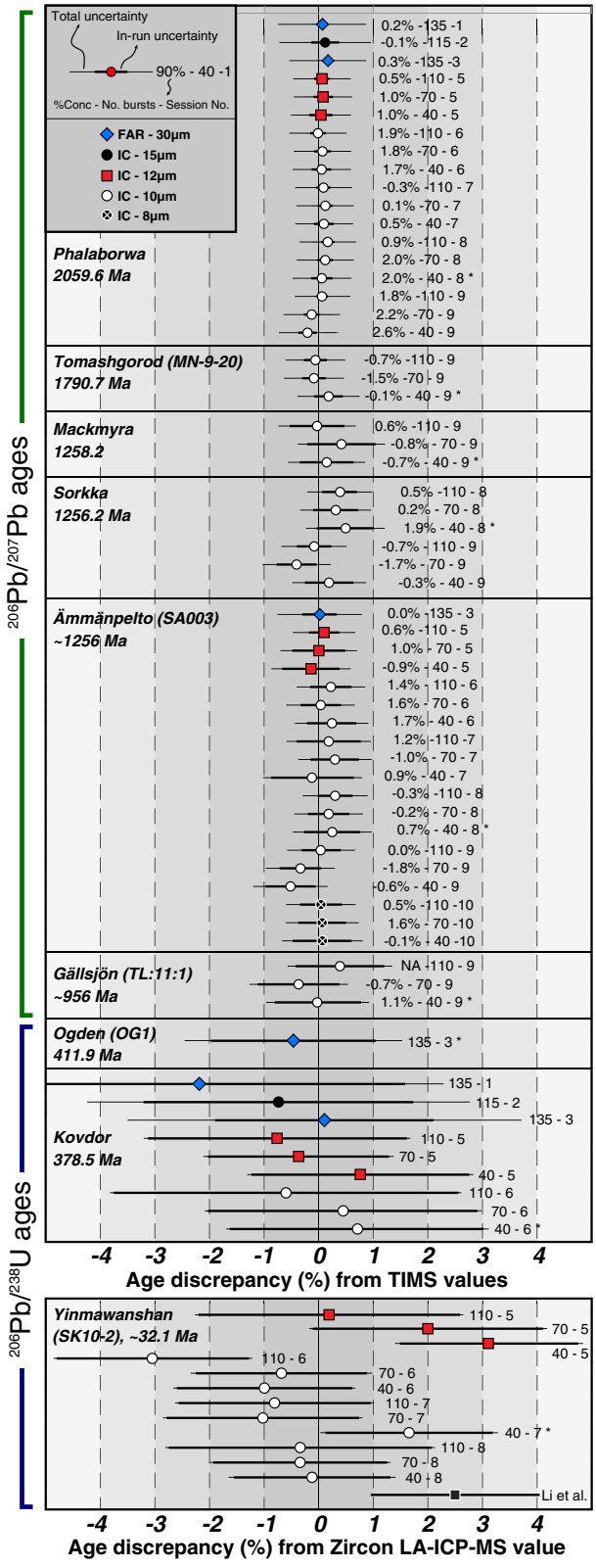

Fig. 9. Comparison of LA-MC-ICP-MS age measurements performed during all our analytical sessions from October 2011 to January 2013 with respect to their previously published values. Offsets are calculated from best age estimates (from TIMS values) as % Offset = 100 * ((TIMS age) − (LA-ICP-MS age) / (TIMS age)). Uncertainties are quoted at 95% confidence, where in-run uncertainties represent weighted means before propagation of primary standard over-dispersion factors, and total uncertainties incorporate over-dispersion (see Section 2.1.4 for details). Results denoted with an asterisk are those for which concordia diagrams are shown in Figs. 8 and 13. Data used to construct this figure is available in the Supplementary material. Solid black data point in the SK10-2 panel is SIMS data from Li et al., (2010).

as a function of time in a pattern that mimics their initial U-zoning profiles. Following a subsequent thermal overprint, these Pb profiles will tend to anneal by diffusive fluxing down their own concentration gradients, inducing Pb* migration from high-U zones towards low-U zones.

The time-scales for diffusive annealing of Pb profiles in zoned zircons have been discussed in detail by Cherniak and Watson (2000). These authors demonstrated that, when not affected by radiation damage, Pb zoning profiles in zircon would not be significantly modified by volume diffusion even during protracted heating episodes at temperatures higher than those typically achieved within the crust (>700 °C). For baddeleyites, this is impossible to quantify at this point given the lack of experimental Pb diffusion data. However, if we accept that the apparent closure temperature of the U–Pb system in baddeleyite is close to that of zircon (Amelin et al., 1999; Soderlund et al., 2004), in a qualitative way our observations seem to imply that Pb-migration within FC-1 crystals was induced by re-heating after the crystals had been significantly affected by radiation damage, or that the operating mechanisms of intracrystalline Pb diffusion in baddeleyite are fundamentally different from those of zircon. Enhanced intra-crystalline Pb* migration in baddeleyite relative to zircon could be a consequence of radiation-induced phase transformations (Valdez et al., 2008), which could generate 'fast-paths' for Pb diffusion along sub-domain grain boundaries. The implantation of Pb* in low-U areas might also provide a feasible explanation to the observation made by Rioux et al. (2010) regarding the frequent reverse discordance measured in Phalaborwa crystals after they have been treated with their chemical-abrasion technique (i.e., low radiation-damaged areas that survive the initial leaching steps could have suffered Pb-gain). For our analytical method, further improvements on the general accuracy of the fractionation uncertainty contributions could be made if a more 'suitable' (less zoned and less affected by Pb-loss) primary standard than FC-1 was calibrated and made available in the future.

6. The limiting effects of out-of-equilibrium ^{231}Pa enrichments on the accuracy of high-precision Precambrian baddeleyite ages

A known source of error for the accurate estimation of U–Th–Pb ages in any mineral system is the potential excess or deficiency of radiogenic Pb that might result from initial disequilibrium concentrations of isotopes intermediate to the U and Th decay chains. A typical example of this phenomenon is the ^{206}Pb excess found in some monazites, produced as a result of excess incorporation of the relatively short-lived ^{230}Th isotope that is intermediate to the ^{238}U–^{206}Pb decay chain (Schärer, 1984). In baddeleyites, it has been observed from trace-element studies that they tend to incorporate very little Th relative to U (e.g., Soderlund et al., 2008), and so deficiency rather that excess of ^{206}Pb is expected as a result. This initial degree of disequilibria is usually fairly small, and because the relative Th concentrations in a crystal can be estimated from the measurement of a longer-lived isotope (i.e., ^{232}Th), this deficiency can easily be accounted for and does not represent an issue for the accurate estimation of ^{206}Pb/^{238}U ages when no other complications such as Pb-loss are present (Amelin and Zaitsev, 2002). On the other hand, for the ^{235}U–^{207}Pb decay-chain, ^{231}Pa can also introduce similar complications, but in this case its excess rather than deficiency is the cause of the problem. Excess initial concentrations of ^{231}Pa have been suggested to be a potential source of primary discordance in some baddeleyites, as its decay produces an equivalent amount of unaccounted ^{207}Pb that affects ^{207}Pb/^{235}U ratios (Crowley and Schmitz, 2009; Hoaglund, 2010). Protactinium has no other naturally occurring isotopes besides 231, and initial enrichments in a closed system will rapidly return to secular equilibrium values so no direct proxies can be used to estimate initial concentrations in crystals older than a ca. 200 ka (Schmitt, 2007). Therefore, the magnitude of initial disequilibria for old crystals cannot be independently quantified. In addition to having an effect for age calculations using the ^{207}Pb/^{235}U ratio,

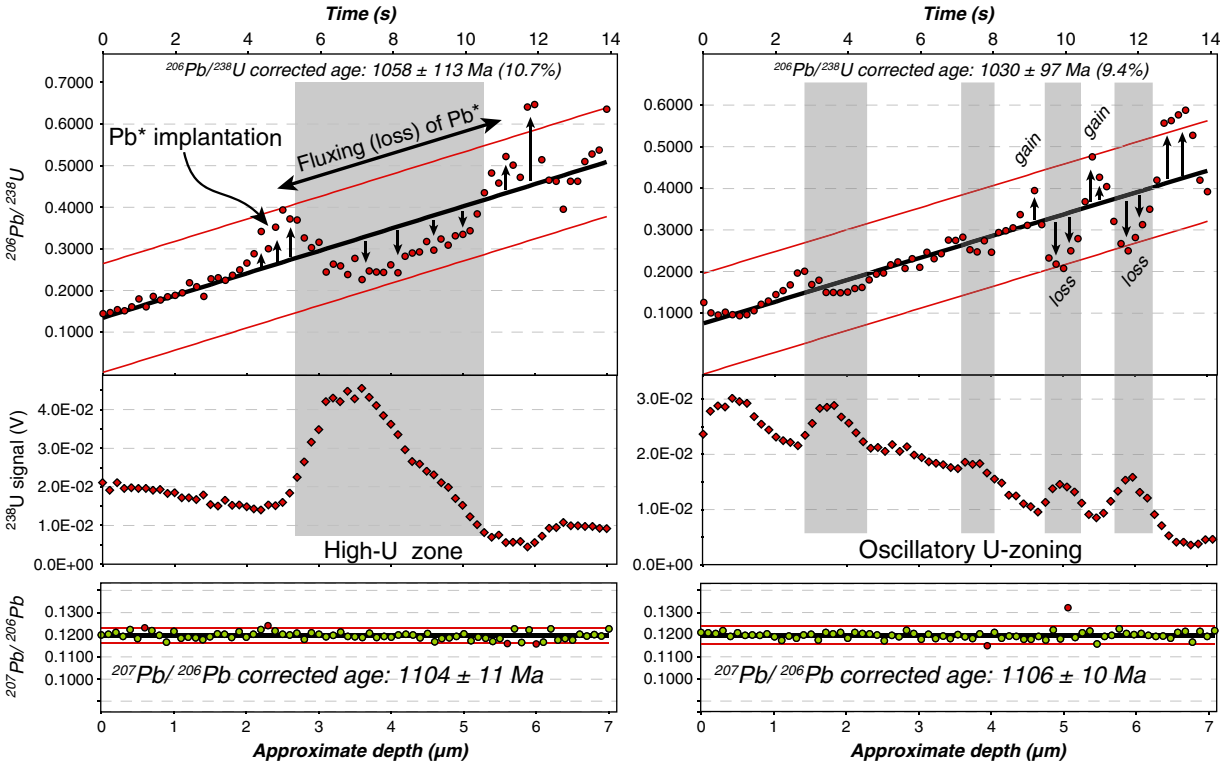

Fig. 10. Examples of individual spot acquisitions on FC-1 crystals showing evidence for internal mobility of radiogenic Pb. Data shown was acquired using a 10 μm spot-diameter. Internal U zoning is evidenced by alternating increases and decreases in the ^{238}U signal intensity (compare this with the gradual decrease typical of unzoned crystals shown in Fig. 1). Subsequent heating events after internal Pb zoning profiles have been developed (by radioactive decay of U) induced diffusive fluxing towards lower Pb – also lower U – concentration zones. Upward- and downward pointing arrows indicate areas affected by Pb gain (higher-than-expected $^{206}Pb/^{238}U$) and Pb loss (lower $^{206}Pb/^{238}U$) in these natural diffusion couples. These FC-1 analyses were corrected for fractionation by treating them as unknowns during reduction and applying the fractionation correction factor derived from neighboring FC-1 measurements as shown in Fig. 4.

excess ^{207}Pb also affects the $^{207}Pb/^{206}Pb$ ratios in a direction of anomalous positive age offset. Fig. 11 illustrates the expected magnitude of anomalous positive shift (in %) on the calculated $^{207}Pb/^{206}Pb$ ages with respect to the 'true' age of a crystal, as a function of the initial degree of ^{231}Pa enrichment expressed as initial $^{235}U/^{231}Pa$ ratio. The gray shaded areas in Fig. 11 are the typical analytical uncertainties that are routinely achieved for the $^{207}Pb/^{206}Pb$ ratio using our LA-ICP-MS method (~0.5 to 2.0%) and those of ID-TIMS (~0.02 to 0.2%). Potential age errors generated by excess ^{231}Pa are, in most cases, not resolvable by LA-ICP-MS dating and therefore the reported $^{207}Pb/^{206}Pb$ ages are likely accurate within the quoted uncertainties. The same does not apply for ID-TIMS dating, however, as the higher level of analytical precision implies that smaller magnitudes of enrichment are readily resolvable and could lead to the erroneous interpretation of high-precision, normally discordant ages. If the obtained ratios for Precambrian baddeleyite samples are concordant (at least in some of the analyzed fractions), then age estimates are most likely accurate within the quoted analytical errors. On the other hand, if the results are normally discordant, there is a possibility for this discordance to be primary and generated by ^{231}Pa enrichment instead of due to Pb-loss, or also by loss of the intermediate daughter product ^{222}Rn. This last mechanism was proposed by Davis and Sutcliffe (2012) in order to explain normally discordant baddeleyite ages from the Logan Sills of the Lake Nipigon area, which show $^{207}Pb/^{206}Pb$ ages that are slightly older than co-existing zircons from the same samples. It should be noted that normal discordance generated by the ^{222}Rn-loss mechanism would explain the relatively younger $^{206}Pb/^{238}U$ and older $^{207}Pb/^{206}Pb$ baddeleyite ages for FC-4b better than ^{231}Pa enrichment alone. Nevertheless, ^{222}Rn-loss would not fit that well with the results obtained by Amelin and Zaitsev (2002) for their Kovdor crystals, and enrichments of the observed magnitude ($^{235}U/^{231}Pa \approx 350$ according to Fig. 11) would be resolvable by TIMS for crystals at least as old as 2.0 Ga (Gray TIMS band in Fig. 11). It should be evident from these potential complexities that care should be exercised in the interpretations of stand-alone, upper-intercept

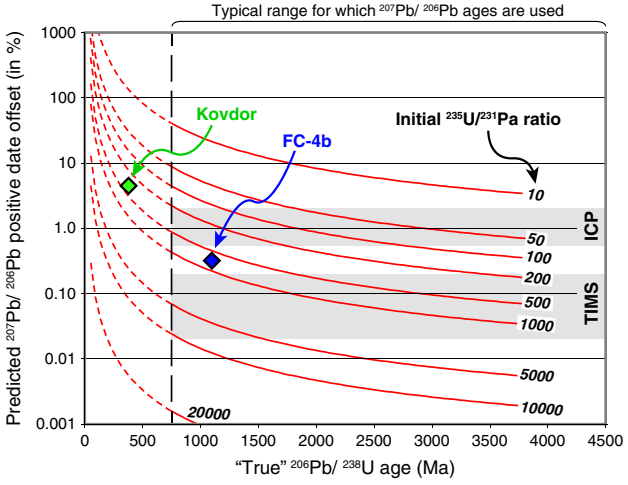

Fig. 11. Theoretically predicted $^{207}Pb/^{206}Pb$ positive date offsets that would be generated in baddeleyites with initial disequilibrium enrichments in 231-Protactinium. Age offsets for Kovdor and FC-4b crystals were calculated using the data of Amelin and Zaitsev (2002) and Hoaglund (2010), respectively. Assuming that their primary normal discordance is all due to ^{231}Pa enrichments, calculated initial $^{235}U/^{231}Pa$ ratios must be in the range of ~350 to 750 (note that $^{235}U/^{231}Pa$ values at secular equilibrium approach ~21520). Grey bands labeled ICP and TIMS represent the range of analytical precision on the $^{207}Pb/^{206}Pb$ ratios (and thus resolving power) that can be achieved with both of these methods.

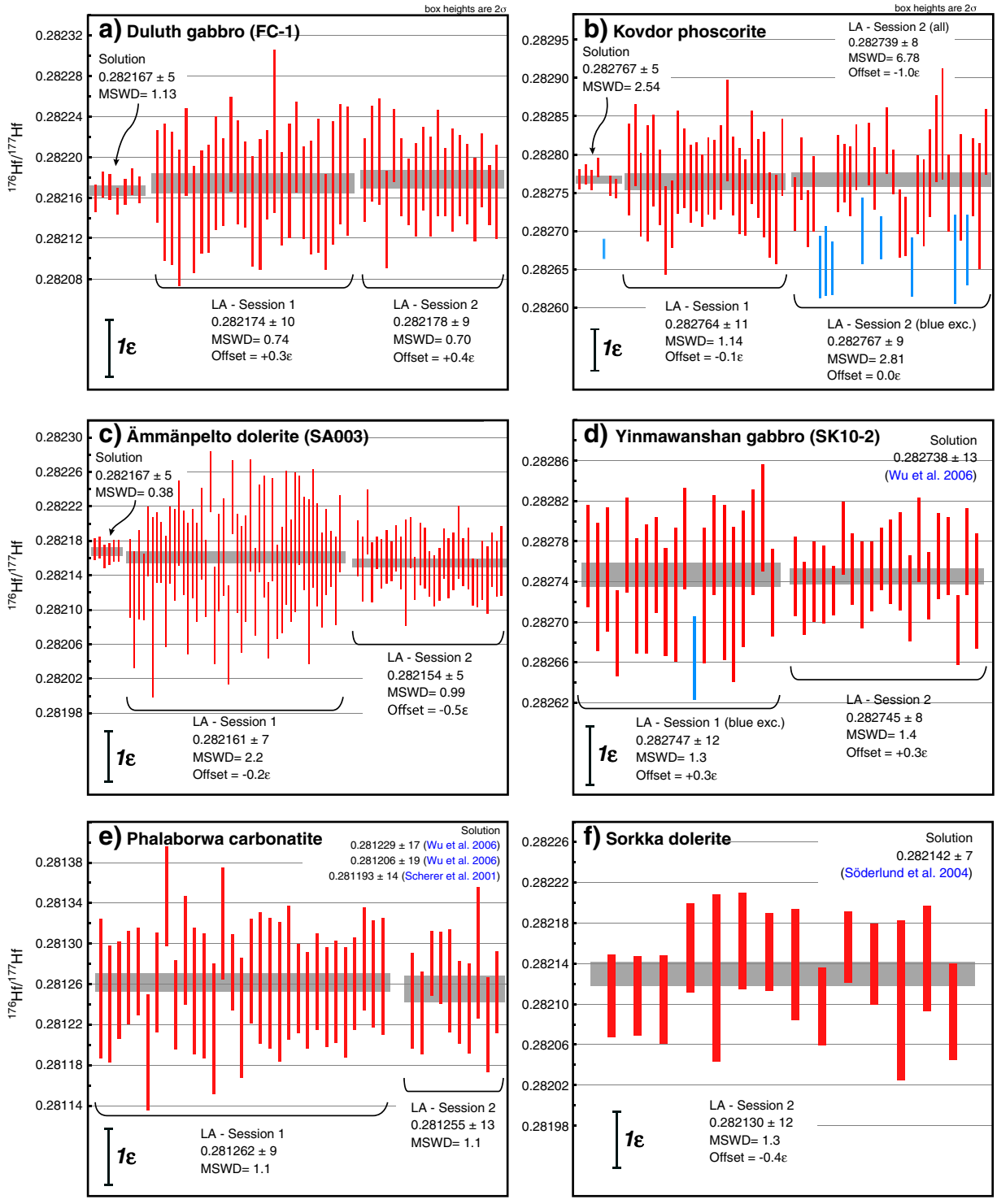

Fig. 12. Summary of all LA Lu–Hf results obtained for reference baddeleyites during the course of our two analytical sessions. Individual error bars represent 2σ standard errors on the mass bias and interference corrected $^{176}Hf/^{177}Hf$ ratios, with an average uncertainty of ±0.000050 (ca. ±1.8 εHf units). Blue bars are data points excluded from the weighted mean calculations. Width of the gray bands is proportional to the uncertainty of the mean for each run. All solution and LA values presented in the figure are modern ratios and have not been age-corrected for ^{176}Hf ingrowth by ^{176}Lu decay.

$^{207}Pb/^{206}Pb$ age data, as the 'true' age of crystallization for the sample in question might lie outside of the quoted levels of analytical uncertainty.

7. Hf isotopic measurements

Similar to the U–Pb results discussed above, we conducted LA Lu–Hf analyses on several reference baddeleyite crystals in order to estimate the overall precision, accuracy and reproducibility of our analytical protocol. Given that many of the samples we used had not been previously characterized by solution-MC-ICP-MS analyses, and such data are the benchmark for accurate Hf isotope ratios (Vervoort et al., 2004; Woodhead and Hergt, 2005; Wu et al., 2006; Cecil et al., 2011; Fisher et al., 2014b), we report new solution results from four of our reference crystals and use them to evaluate the laser data. The solution-MC-ICP-

MS results are presented in Table 2 and the complete dataset for the LA-MC-ICP-MS results is available as repository material. All uncertainties to the reported weighted mean values are quoted at a 2σ confidence level unless otherwise noted.

7.1. Duluth gabbro (FC-1)

We performed eight solution analyses in crystals from this important locality for which baddeleyite Hf results were previously unavailable. Seven of these measurements yield a weighted mean of 0.282167 ± 5 (Fig. 12a) and one aliquot was discarded due to relatively high residual interference ratios. Zircons from this locality had been previously studied for Hf isotopic ratios via solution-MC-ICP-MS by Woodhead and Hergt (2005) and Fisher et al. (2014b), obtaining mean $^{176}Hf/^{177}Hf$ values of 0.282184 ± 16 and 0.282182 ± 12, respectively. This discrepancy between zircons and baddeleyites is partially reconciled after Lu-decay age corrections are applied to the data; when recalculated at crystallization age (1098 Ma) the initial $^{176}Hf/^{177}Hf$ composition for the zircon data of Fisher et al. (2014b) is 0.282162 ± 12, for the zircon data of Woodhead and Hergt (2005) is 0.282158 ± 16, and our new baddeleyite analyses yield a value of 0.282165 ± 5. Note that the $^{176}Lu/^{177}Hf$ values reported by Woodhead and Hergt (2005) and Fisher et al. (2014b) for zircon analyses show mean values of 0.001262 and 0.001009 ± 132, which is over an order of magnitude higher than those reported here for baddeleyite crystals (average $^{176}Lu/^{177}Hf$ = 0.000105). Although the corrected initial $^{176}Hf/^{177}Hf$ values for zircons and baddeleyites agree within analytical uncertainty, it is evident that the zircon data require a more significant radiogenic-ingrowth correction than baddeleyite. Therefore, in samples that lack any zircon or contain both minerals, baddeleyite is an equally or more reliable phase than zircon that can be used to obtain Hf isotopic compositions at time of crystallization. Our LA-MC-ICP-MS weighted average $^{176}Hf/^{177}Hf$ values for this sample are accurate to within 0.4 εHf units for both analytical sessions.

7.2. Kovdor phoscorite

Seven solution analyses were performed on fragments from a single Kovdor megacryst, all of them yielding <0.03% total interference ratios in the 176 mass. Six of these runs are consistent with a $^{176}Hf/^{177}Hf$ weighted-mean average of 0.282767 ± 5 while one of the aliquots has a significantly lower value of 0.282677 and was excluded from the average calculations (Fig. 12b). This last aliquot was analyzed for a second time and the same value was reproduced, thus discarding the possibility of a spurious run. This anomalous value, in addition to the slightly elevated MSWD value of the aforementioned weighted-mean (MSWD = 2.44), suggests that the scatter observed in this Kovdor crystal is likely a consequence of real isotopic heterogeneity within this single crystal as it cannot be explained by our estimated analytical uncertainties alone. The laser results also provide support for this conclusion, and it is evident from the second LA session of Kovdor that the obtained ratios show a much larger degree of scatter in $^{176}Hf/^{177}Hf$ than any of the other samples we have analyzed so far. Also, all the apparent 'outlier' analyses from this session yield values that are lower than the mean and are in close agreement with the excluded solution aliquot. A crystal with REE concentrations as low as Kovdor would be ideal for quantifying instrumental biases for Hf isotopes using LA-MC-ICP-MS but, unfortunately, these preliminary results may preclude the use of this crystal as a potential reference material given its variable $^{176}Hf/^{177}Hf$ ratios. More detailed analyses coupled with careful grain imaging are necessary to better address this observation for other Kovdor crystals in the future.

7.3. Ämmänpelto dolerite (SA-003)

Baddeleyites from this locality had not been previously studied for Hf isotope systematics, but they bear close resemblance to other dykes and sills of the Central Scandinavian Dolerite Group studied in the past by Soderlund et al. (2005; 2006). From the eight solution analyses performed, six had clean Hf separations and yielded a modern $^{176}Hf/^{177}Hf$ ratio of 0.282167 ± 5 (MSWD = 0.37). $^{176}Lu/^{177}Hf$ values estimated from the SC-ICP-MS runs shown in Table 2 indicate that crystals from this dolerite have significantly higher REE concentrations compared to other samples analyzed during this study. This observation is also confirmed by the LA-MC-ICP-MS results, and the range of Yb concentrations measured was found to be anywhere from ~5 to 28% in $^{176}Yb/(^{176}Yb + ^{176}Hf)$ interference. From our two LA sessions, we obtained $^{176}Hf/^{177}Hf$ values of 0.282161 ± 7 (n = 48, MSWD = 2.2) and 0.282154 ± 5 (n = 31, MSWD = 0.99), respectively. These ratios indicate offsets within 0.5 εHf units from the measured solution values (Fig. 12c).

7.4. Yinmawanshan gabbro (SK10-2)

Solution and LA-MC-ICP-MS Hf results for baddeleyites from this gabbro were reported by Wu et al. (2006) and based on their results they recommend a modern $^{176}Hf/^{177}Hf$ reference ratio of 0.282738 ± 13. From our two LA sessions, we obtained ratios of 0.282747 ± 12 (n = 19, MSWD = 1.3) and 0.282745 ± 8 (n = 20, MSWD = 1.4), respectively, indicating offsets within 0.4 εHf units from the solution value for both runs. One spot analysis from session one was discarded based on a two-sigma outlier filter (Fig. 12d). Yb interferences to ^{176}Hf measured by us range from ~4 to ~20% ($^{176}Yb/^{177}Hf$ ratios between 0.010393 and 0.071414). These are significantly higher than those reported by Wu et al. (2006) but still result in a corrected $^{176}Hf/^{177}Hf$ value that is in very good agreement with their solution results.

7.5. Phalaborwa carbonatite

The Phalaborwa carbonatitic complex is probably the best-studied locality in terms of baddeleyite Hf isotope systematics. Solution-MC-ICP-MS analyses have been published by Scherer et al. (2001) and Wu et al. (2006). Scherer et al. (2001) obtained modern ratios of 0.281193 ± 14 and 0.281181 ± 14 from two individual spiked and unspiked runs, with a very low $^{176}Lu/^{177}Hf$ ratio of 0.000005; no Yb concentrations or $^{176}Yb/^{177}Hf$ ratios were reported by these authors. Wu et al. (2006) measured several aliquots for two different baddeleyite megacrysts, obtaining $^{176}Hf/^{177}Hf$ ratios of 0.281229 ± 11 (n = 13, MSWD = 8.6) and 0.281206 ± 19 (n = 20, MSWD = 18). The differences in $^{176}Hf/^{177}Hf$ results obtained by these two studies, along with the high MSWD values for the weighted means reported by Wu et al. (2006), indicate that there is significant inter- and intra-grain variability in Hf isotopic ratios for baddeleyite megacrysts from this locality. This observation was later confirmed by LA-MC-ICP-MS measurements, and $^{176}Hf/^{177}Hf$ values found in the literature range anywhere from 0.281184 ± 6 to 0.281267 ± 37 (Wu et al., 2010; 2011; Xie LieWen et al., 2008). During our two LA sessions (Fig. 12e) we obtained weighted-mean $^{176}Hf/^{177}Hf$ ratios of 0.281262 ± 9 (n = 31, MSWD = 1.1) and 0.281255 ± 13 (n = 10, MSWD = 1.1). These values are within the range of previously published results, but since we did not conduct any solution analyses from this Phalaborwa crystal we cannot estimate the accuracy of our LA-MC-ICP-MS results.

7.6. Sorkka dolerite

Baddeleyite Hf analyses from the Sorkka dolerite were used by Söderlund et al. (2004) to calculate the decay constant of ^{176}Lu. From a mineral Lu–Hf isochron they deduced an initial $^{176}Hf/^{177}Hf$ ratio of 0.282142 ± 7 for the parental melt of this dolerite, and the baddeleyite fractions displayed modern ratios ca. 0.282144. LA-MC-ICP-MS results measured in Session 2 have an average modern value of 0.282130 ± 12 (n = 14, MSWD = 1.3), indicating an offset of −0.5 εHf units

from the published solution value (Fig. 12f). Considering the fact that these Sorkka crystals display large Yb interferences up to 38% on the measured $^{176}(Yb + Lu + Hf)/^{177}Hf$ ratios, and no apparent $^{176}Hf/^{177}Hf$ vs. $^{176}Yb/^{177}Hf$ trends are observed in the data, we consider the agreement between our laser data and the solution results to be an indication of the robust Yb interference corrections that are achieved by our procedure.

8. Applied example: the age and Hf isotopic composition of the Ogden gabbro — Southern Appalachians

The Ogden pluton of the Southern Appalachians is a mafic intrusive body consisting entirely of gabbronorite with distinct hornblende- and olivine-rich facies (McSween, 1981), whose crystallization age has been estimated at 406 ± 32 Ma by a Sm–Nd mineral isochron (McSween et al., 1984). Field relationships indicate that this gabbro is intrusive into slightly older (ca. 580 to 520 Ma) metagabbros and paragneisses of the Charlotte Belt (Butler, 1966), and is associated with other gabbroic to syenitic plutons in the Carolinia terrane that also yield Lower Devonian ages by the Sm–Nd method (the Concord-Salisbury Plutonic Suite; McSween et al., 1984). Mineral separates from a fresh hornblende gabbro sample (N34°49′36.7″, W81°05′29.9″) yielded abundant baddeleyite and zircon crystals with subhedral to anhedral sub-rounded shapes, reaching up to 120 μm in diameter. Baddeleyite crystals were analyzed for U–Pb geochronology and Hf isotopes using our LA-MC-ICP-MS methods before subsequent CA-TIMS and solution-MC-ICP-MS Hf results were obtained (Tables 2 and 3). Fig. 13a shows the CA-TIMS U–Pb results, which constraint the baddeleyite crystallization age from the Ogden gabbro to the Lower Devonian Lochkovian stage at 411.91 ± 0.25(0.32)[0.54] Ma and Fig. 13b shows the excellent agreement of the LA-MC-ICP-MS results obtained with our analytical protocols using FC-1 baddeleyite to correct for U–Pb fractionation (red ellipses), yielding an age of 410.0 ± (6.2) [8.2] Ma. This demonstrates the accuracy of our $^{206}Pb/^{238}U$ fractionation–correction procedures for dating Phanerozoic samples. Along with the baddeleyite crystals, we mounted and analyzed fragments of our Sri Lanka (SL2) in-house zircon standard (Gehrels et al., 2008) and used those to correct the same baddeleyite dataset just to illustrate the results of a non-matrix-matched reduction procedure. The gray ellipses in Fig. 13b are the raw, uncorrected data, which yields a $^{206}Pb/^{238}U$ weighted-mean date of 520.7 ± 7.8 Ma, and the black ellipses are the zircon-corrected data, which produce another false

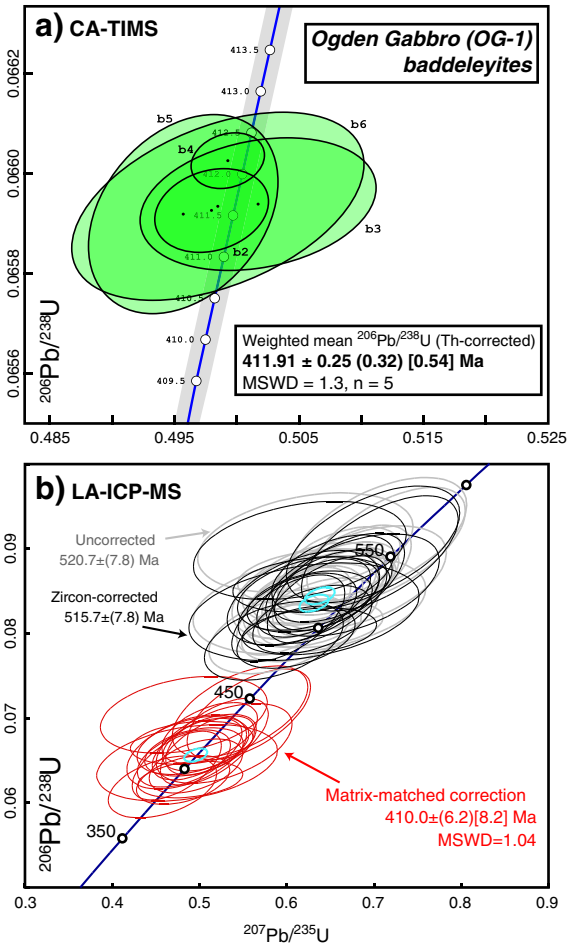

Fig. 13. CA-TIMS and LA-ICP-MS U-Pb results for baddeleyites of the Ogden gabbro. Red ellipses are results calculated using our matrix-matched $^{206}Pb/^{238}U$ fractionation correction procedure using FC-1 baddeleyite; black ellipses are the raw fractionation-uncorrected data and gray ellipses are the zircon-corrected data (see text for details). The gray ellipses exemplify the inadequacy of using zircon crystals as primary fractionation reference material to correct for baddeleyite instrumental fractionations. Uncertainty brackets are quoted according to the methods described for TIMS and LA-ICP-MS in Sections 2.2 and 2.1.4, respectively.

Table 3
CA-TIMS U–Pb results for baddeleyites of the Ogden Gabbro.

Fraction	Dates (Ma)										Composition				Isotopic ratios						
	$^{206}Pb/^{238}U$ <Th>[a]	±2σ abs	$^{206}Pb/^{238}U$ [b]	±2σ abs	$^{206}Pb/^{238}U$ [b]	±2σ abs	$^{207}Pb/^{238}U$ [b]	±2σ abs	Corr. coef.	% disc [c]	Pb* (pg) [d]	Pbc (pg) [e]	Pb*/Pbc [f]	Th/U [g]	$^{206}Pb/^{204}Pb$ [h]	$^{206}Pb/^{238}U$ [i]	±2σ %	$^{207}Pb/^{235}U$ [i]	±2σ %	$^{207}Pb/^{206}Pb$ [i]	±2σ %
Baddeleyite																					
b2	411.11	0.50	411.01	0.50	409.4	3.1	401	20	0.329	−2.61	6.04	0.40	15.2	0.00	1067	0.065834	0.13	0.4967	0.93	0.05474	0.90
b3	411.59	0.80	411.48	0.80	412.8	6.4	420	41	0.247	2.09	4.41	0.67	6.6	0.00	472	0.06591	0.2	0.5016	1.9	0.0552	1.8
b4	412.25	0.34	412.15	0.34	411.5	2.0	408	13	0.243	−1.03	10.3	0.44	23.2	0.00	1617	0.066023	0.084	0.4997	0.59	0.05492	0.58
b5	412.49	0.98	412.39	0.98	411.1	5.2	404	33	0.366	−2.14	4.89	0.52	9.4	0.00	671	0.06606	0.25	0.4991	1.5	0.05482	1.5
b6	411.7	1.1	411.6	1.1	410.8	7.9	406	50	0.446	−1.39	6.39	1.10	5.8	0.00	418	0.06593	0.29	0.499	2.4	0.0549	2.2

[a] Corrected for initial Th/U disequilibrium using radiogenic ^{208}Pb and Th/U[magma] = 2.80.
[b] Isotopic dates calculated using the decay constants λ238 = 1.55125E-10 and λ235 = 9.8485E-10 (Jaffey et al. 1971).
[c] % discordance = 100 − (100 * (^{206}Pb / ^{238}U date) / (^{207}Pb / ^{206}Pb date)).
[d] Total mass of radiogenic Pb.
[e] Total mass of common Pb.
[f] Ratio of radiogenic Pb (including ^{208}Pb) to common Pb.
[g] Th contents calculated from radiogenic ^{208}Pb and the $^{207}Pb/^{206}Pb$ date of the sample, assuming concordance between the U–Th and Pb systems.
[h] Measured ratio corrected for fractionation and spike contribution only.
[i] Measured ratio corrected for fractionation, tracer and blank.

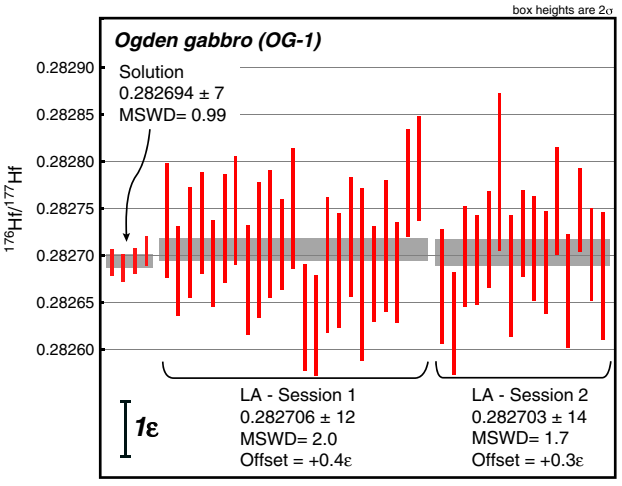

Fig. 14. Solution and laser ablation Lu–Hf results for baddeleyites of the Ogden gabbro. Values shown are modern measured ratios and have not been age-corrected for ^{176}Hf ingrowth by ^{176}Lu decay.

date of 515.7 ± 7.8 Ma. These results clearly demonstrate the inadequacy of using zircon as a fractionation monitor to correct for baddeleyite LA-ICP-MS U–Pb data as is commonly found in the literature (Renna et al., 2011; Xie LieWen et al., 2008).

Using our Lu–Hf approach, ratios measured during session one yielded an average modern ^{176}Hf/^{177}Hf value of 0.282706 ± 12 (MSWD = 2.0, n = 23) and those from session two averaged 0.282703 ± 14 (MSWD = 1.7, n = 15). Calculated ^{176}Hf/^{177}Hf ratios at the time of crystallization are undistinguishable from the modern ratios, owing to the young age of this gabbro and the low Lu concentrations of these baddeleyites. These results yield initial εHf values of 6.4 ± 0.6 and 6.3 ± 0.7, respectively, and are in excellent agreement with the subsequent solution measurements which yielded an average modern ^{176}Hf/^{177}Hf value of 0.282694 ± 7 (n = 4, MSWD = 0.99) and $\varepsilon Hf_{(t)}$ of 5.9 ± 0.3 (Fig. 14).

The Concord-Salisbury Plutonic Suite (CSPS) appears mostly unmetamorphosed, and intrudes metamafic and metasedimentary rocks of the Battleground Formation (Hibbard et al. 2006). Based on this observation the CSPS has been interpreted to post-date the main episode of deformation of the Carolinia terrane, which took place in Late Ordovician to Silurian times as this peri-Gondwanan crustal fragment accreted to the Appalachian Piedmont during the Salinian Orogeny (Hibbard et al., 2007; van Staal, 2007; Nance et al., 2010). The new geochronological and isotopic constraints from the Ogden gabbro further refine the chronology of the CSPS, restrict significant upper Paleozoic metamorphism and deformation to pre-Lower Devonian times, and attest for the role of juvenile, mantle-derived magmatic input for the genesis of the early-Acadian magmatism of the Southern Appalachians.

There are, to date, very few published TIMS U–Pb results for Phanerozoic baddeleyites as previous studies have mostly focused on studying Precambrian mafic dyke-swarms (e.g., Hanski et al., 2006; Ernst et al., 2013). We suggest that baddeleyite crystals from the Ogden gabbro can potentially be of use as a secondary standard for inter-laboratory comparisons and to monitor the accuracy of LA-ICP-MS and SIMS Pb/U fractionation corrections. Mineral separates, consisting of both baddeleyite and zircon from this intrusion, can be obtained by request from the author or by contacting the ALC lab.

9. Conclusions

We present a method for LA-ICP-MS U–Pb dating of baddeleyites which is capable of routinely producing ages with accuracy and precision ~1.0–2.5%, which is comparable to what can be achieved in zircon by using similar analytical techniques. These results are reproducible with spot sizes ranging from 30 μm down to 8 μm in diameter, excavating pits of ca. 2.8, 5.0 or 7.7 μm in depth. We found the pre-ablation cleaning technique to be helpful in reducing surficial common-Pb contamination of the analyses especially for the short-burst acquisitions, significantly enhancing the accuracy of the ^{207}Pb/^{206}Pb ratios and improving concordance. Our new low-volume analytical routine represents a significant improvement over the typical volumes sampled by conventional LA-ICP-MS U–Pb geochronology, while still retaining the ability to perform robust down-pit fractionation corrections that allow us to identify elemental/isotopic zoning complexities to a sub-micron scale.

Experiments aimed at addressing the potential variability in instrumental fractionation introduced by crystallographic-orientation effects suggest that this phenomenon does not constitute a significant impediment to the accuracy with which Phanerozoic baddeleyites can be dated by LA-ICP-MS, as demonstrated by the accurate ^{206}Pb/^{238}U ages obtained from crystals of the Ogden, Kovdor and Yinmawanshan localities. Further improvement in the precision of the method can be achieved by the introduction of a more suitable primary standard that does not suffer from the strong uranium zonation and intra-grain Pb mobility complexities that we have described from FC-1 baddeleyites.

In addition to the U–Pb geochronologic results, we present high-precision solution-MC-ICP-MS Hf isotopic results from four baddeleyite localities that can be used as reference crystals for addressing the accuracy of LA-MC-ICP-MS Hf data. We obtained modern ^{176}Hf/^{177}Hf ratios of 0.282167 ± 5 for FC-1 baddeleyites, 0.282767 ± 5 for a crystal from a Kovdor phoscorite, 0.282167 ± 5 for the Ämmänpelto dolerite (SA-003), and 0.282694 ± 7 for the Ogden gabbro. Based on these new results we are able to demonstrate that our LA-MC-ICP-MS Lu–Hf routine is capable of producing weighted average ^{176}Hf/^{177}Hf ratios that are accurate to within 0.5 εHf units with respect to their solution values.

The last thirty years have seen a rapid and steady increase in the number of publications that utilize baddeleyite U–Pb ages to date the emplacement of mafic and other silica-undersaturated igneous rocks (Fig. 1 in Söderlund et al., 2013). With applications in the fields of igneous petrology, tectonics, crust and mantle evolution, and supercontinent reconstructions by using the LIP record, among others, the ability to rapidly and accurately obtain U–Pb–Hf information from baddeleyites by LA-MC-ICP-MS will prove to be a very useful tool for several fields of the Earth Sciences in the near future.

Acknowledgments

The authors would like to acknowledge the help from several people that contributed with the samples that made this research possible: Jonathan Patchett and Olavi Kouvo for crystals from the Ämmänpelto dolerite, Ulf Söderlund for samples from the Sorkka, Tomashgorod, Mackmyra and Gällsjön dolerites, Matthew Huebner and Bob Hatcher for crystals and rock samples from the Ogden gabbro, Fu-Yuan Wu for crystals from the Yinmawanshan gabbro, and Ellen de Kock and Stuart Thomson for crystals from the Phalaborwa carbonatite. Diane Wilford and Charles Knack provided invaluable help during the Hf-solution analyses at WSU. Tom Milster and Melissa Zaverton are acknowledged for their help with the optical interferometry measurements. The ICP-MS and SEM facilities at the Arizona Laserchron center are partially funded by NSF-EAR Grants #1338583 and #0732436. This research also benefited from NSF grant #1144521. The manuscript was enriched by discussions and comments to an early version of the text made by Kendra Murray, Alex Pullen, Mark Pecha and Martin Pepper. Additional comments made by Axel Schmitt, editor Klaus Mezger and two anonymous reviewers helped improve the final version of the text and figures.

Appendix A. Supplementary data

Supplementary data to this article can be found online at http://dx.doi.org/10.1016/j.chemgeo.2014.07.011.

References

Amelin, Y., Zaitsev, A.N., 2002. Precise geochronology of phoscorites and carbonatites: the critical role of U-series disequilibrium in age interpretations. Geochim. Cosmochim. Acta 66, 2399–2419.

Amelin, Y., Li, C., Naldrett, A.J., 1999. Geochronology of the Voisey's Bay intrusion, Labrador, Canada, by precise U–Pb dating of coexisting baddeleyite, zircon, and apatite. Lithos 47, 33–51.

Bachmann, F., Hielscher, R., Schaeben, H., 2010. Texture analysis with MTEX — free and open source software toolbox. Solid State Phenom. 160, 63–68.

Beckman, V., Möller, C., Söderlund, U., Cofu, F., Pallon, J., Chamberlain, K.R., 2014. Metamorphic zircon formation at the transition from gabbro to eclogite in Trollheimen-Surnadalen, Norwegian Caledonides. Geological Society of London, Special Publications. In: Corfu, F., Gasser, D., Chew, D.M. (Eds.), New Perspectives on the Caledonides of Scandinavia and Related Areas. Special Publications, 390. http://dx.doi.org/10.1144/SP390.26 (23 pp.).

Bogdanova, S.V., Gintov, O.B., Kurlovich, D.M., Lubnina, N.V., Nilsson, M.K.M., Orlyuk, M.I., Pashkevich, I.K., Shumlyanskyy, L.V., Starostenko, V.I., 2013. Late Palaeoproterozoic mafic dyking in the Ukrainian Shield of Volgo-Sarmatia caused by rotation during the assembly of supercontinent Columbia (Nuna). Lithos 174, 196–216.

Bowring, J.F., McLean, N.M., Walker, J.D., Bowring, S.A., 2008. Building cyberinfrastructure for geochronology: software engineering meets geochemistry. Abstr. Programs - Geol. Soc. Am. 40 (6), 136.

Bowring, J., Horstwood, M., Gehrels, G.E., 2013. Resolving bias in laser ablation geochronology. Eos, Trans. Am. Geophys. Union 94 (24), 217.

Butler, J.R., 1966. Geology and mineral resources of York County, South Carolina. South Carolina State Development Board Bulletin 33 Plate 1.

Cecil, M.R., Gehrels, G., Ducea, M.N., Patchett, P.J., 2011. U–Pb–Hf characterization of the central Coast Mountains batholith: implications for petrogenesis and crustal architecture. Lithosphere 3, 247–260.

Chamberlain, K.R., Schmitt, A.K., Swapp, S.M., Harrison, T.M., Swoboda-Colberg, N., Bleeker, W., Peterson, T.D., Jefferson, C.W., Khudoley, A.K., 2010. In situ U–Pb SIMS (IN-SIMS) micro-baddeleyite dating of mafic rocks: method with examples. Precambrian Res. 183, 379–387.

Chang, Z., Vervoort, J.D., McClelland, W.C., Knaack, C., 2006. U–Pb dating of zircon by LA-ICP-MS. Geochem. Geophys. Geosyst. 7, Q05009.

Cherniak, D.J., Watson, E.B., 2000. Pb diffusion in zircon. Chem. Geol. 172 (1–2), 5–24.

Cherniak, D.J., Lanford, W.A., Ryerson, F.J., 1991. Lead diffusion in apatite and zircon using ion implantation and Rutherford Backscattering techniques. Geochim. Cosmochim. Acta 55 (6), 1663–1673.

Cottle, J.M., Horstwood, M.S.A., Parrish, R.R., 2009. A new approach to single shot laser ablation analysis and its application to in situ Pb/U geochronology. J. Anal. At. Spectrom. 24, 1355.

Cottle, J.M., Kylander-Clark, A.R., Vrijmoed, J.C., 2012. U–Th/Pb geochronology of detrital zircon and monazite by single shot laser ablation inductively coupled plasma mass spectrometry (SS-LA-ICPMS). Chem. Geol. 332–333, 136–147.

Crowley, J.L., Schmitz, M.D., 2009. A precise comparison of U–Pb dates from baddeleyite and zircon: evidence for excess 207Pb in baddeleyite. Eos, Trans. Am. Geophys. Union 90 (52), V53B-06.

Davidson, A., van Breemen, O., 1988. Baddeleyite–zircon relationships in coronitic metagabbro, Grenville Province, Ontario: implications for geochronology. Contrib. Mineral. Petrol. 100, 291–299.

Davis, D.W., Sutcliffe, R.H., 2012. U-Pb ages from the Nipigon plate and northern Lake Superior. Geological Society of America Bulletin 96 (12), 1572–1579.

Ernst, R.E., Bleeker, W., Soderlund, U., Kerr, A.C., 2013. Large Igneous Provinces and supercontinents: toward completing the plate tectonic revolution. Lithos 174, 1–14.

Fisher, C.M., Hanchar, J.M., Samson, S.D., Dhuime, B., Blichert-Toft, J., Vervoort, J.D., Lam, R., 2011. Synthetic zircon doped with hafnium and rare earth elements: a reference material for in situ hafnium isotope analysis. Chem. Geol. 286, 32–47.

Fisher, C.M., Vervoort, J.D., Hanchar, J.M., 2014a. Guidelines for reporting zircon Hf isotopic data by LA-MC-ICPMS and potential pitfalls in the interpretation of these data. Chem. Geol. 363, 125–133.

Fisher, C.M., Vervoort, J.D., DuFrane, S.A., 2014b. Accurate Hf isotope determinations of complex zircons using the "laser ablation split stream" method. Geochem. Geophys. Geosyst. 15, GC004962.

Frei, D., Gerdes, A., 2009. Precise and accurate in situ U–Pb dating of zircon with high sample throughput by automated LA-SF-ICP-MS. Chem. Geol. 261, 261–270.

Gehrels, G.E., Valencia, V.A., Ruiz, J., 2008. Enhanced precision, accuracy, efficiency, and spatial resolution of U–Pb ages by laser ablation-multicollector-inductively coupled plasma-mass spectrometry. Geochem. Geophys. Geosyst. 9, Q03017.

Gehrels, G.E., Rusmore, M., Woodsworth, G., Crawford, M., Andronicos, C., Hollister, L., Patchett, J., Ducea, M., Butler, R., Klepeis, K., Davidson, C., Friedman, R., Haggart, J., Mahoney, B., Crawford, W., Pearson, D., Girardi, J., 2009. U–Th–Pb geochronology of the Coast Mountains batholith in north-coastal British Columbia: constraints on age and tectonic evolution. Geol. Soc. Am. Bull. 121 (9/10), 1341–1361.

Geisler, T., Pidgeon, R.T., van Bronswijk, W., Kurtz, R., 2002. Transport of uranium, thorium, and lead in metamict zircon under low-temperature hydrothermal conditions. Chemical Geology 191, 141–154.

Griffin, W.L., Pearson, N.J., Belousova, E., Jackson, S.E., van Achterbergh, E., O'Reilly, S.Y., Shee, S.R., 2000. The Hf isotope composition of cratonic mantle: LAM-MC-ICPMS analysis of zircon megacrysts in kimberlites. Geochim. Cosmochim. Acta 64, 133–147.

Hann, R.E., Suitch, P.R., Pentecost, J.L., 1985. Monoclinic crystal structures of ZrO_2 and HfO_2 refined from X-ray powder diffraction data. J. Am. Ceram. Soc. 68, C285–C286.

Hanski, E., Mertanen, S., Rämö, T., Vuollo, J., 2006. Dyke swarms — time markers of crustal evolution. Selected Papers of the Fifth International Dyke Conference in Finland, Rovaniemi, Finland, 31 July–3 Aug 2005 & Fourth International Dyke Conference, Kwazulu-Natal, South Africa 26–29 June 2001.

Heaman, L.M., 2009. The application of U–Pb geochronology to mafic, ultramafic and alkaline rocks: an evaluation of three mineral standards. Chem. Geol. 261, 43–52.

Heaman, L., Lecheminant, A., 1993. Paragenesis and U–Pb systematics of Baddeleyite (ZrO_2). Chem. Geol. 110, 95–126.

Hibbard, J.P., van Staal, C.R., Rankin, D.W., Williams, H., 2006. Lithotectonic map of the Appalachian orogen, Canada - United States of America: Geological Survey of Canada Map 02096A, 2 sheets, scale 1:1,500,000.

Hibbard, J.P., Van Staal, C.R., Rankin, D.W., 2007. A comparative analysis of pre-Silurlan crustal building blocks of the northern and the southern Appalachian orogen. Am. J. Sci. 307, 23–45.

Hoaglund, S., 2010. U–Pb Geochronology of the Duluth Complex and Related Hypabyssal Intrusions: Investigating the Emplacement History of a Large Multiphase Intrusive Complex Related to the 1.1 Ga Midcontinent Rift(M.Sc. Thesis) University of Minnesota (103 pages).

Horn, I., Rudnick, R.L., McDonough, W.F., 2000. Precise elemental and isotope ratio determination by simultaneous solution nebulization and laser ablation-ICP-MS: application to U–Pb geochronology. Chem. Geol. 164, 281–301.

Horstwood, M., 2008. Data reduction strategies, uncertainty assessment and resolution of LA-(MC)-ICP-MS isotope data. In: Sylvester, P. (Ed.), Laser Ablation ICP-MS in the Earth Sciences: Current Practices and Outstanding Issues. Mineralogical Association of Canada short course series, 40, pp. 283–300.

Jackson, S.E., Longerich, H.P., Dunning, G.R., Fryer, B.J., 1992. The application of laser-ablation microprobe-inductively coupled plasma-mass spectrometry (LAM-ICP-MS) to in situ trace-element determinations in minerals. Can. Mineral. 30, 1049.

Jaffey, A.H., Flynn, K.F., Glendenin, L.E., Bentley, W.C., Essling, A.M., 1971. Precision measurement of half-lives and specific activities of ^{235}U and ^{238}U. Phys. Rev. C. 4, 1889–1906.

Johnston, S., Gehrels, G., Valencia, V., Ruiz, J., 2009. Small-volume U–Pb zircon geochronology by laser ablation-multicollector-ICP-MS. Chem. Geol. 259, 218–229.

Kemp, A.I.S., Foster, G.L., Schersten, A., Whitehouse, M.J., Darling, J., Storey, C., 2009. Concurrent Pb–Hf isotope analysis of zircon by laser ablation multi-collector ICP-MS, with implications for the crustal evolution of Greenland and the Himalayas. Chem. Geol. 261, 244–260.

Kita, N.T., Huberty, J.M., Kozdon, R., Beard, B.L., Valley, J.W., 2010. High-precision SIMS oxygen, sulfur and iron stable isotope analyses of geological materials: accuracy, surface topography and crystal orientation. Surf. Interface Anal. 43, 427–431.

Klemme, S., Meyer, H.-P., 2003. Trace element partitioning between baddeleyite and carbonatite melt at high pressures and high temperatures. Chem. Geol. 199, 233–242.

Kosler, J., Sylvester, P.J., 2003. Present trends and the future of zircon in geochronology: laser ablation ICPMS. In: Hanchar, J.M., Hoskin, P.W.O. (Eds.), Zircon. Reviews in Mineralogy and Geochemistry, vol. 53, pp. 243–275.

Kosler, J., Slama, J., Belousova, E., Corfu, F., Gehrels, G.E., Gerdes, A., Horstwood, M.S.A., Sircombe, K.N., Sylvester, P.J., Tiepolo, M., Whitehouse, M.J., Woodhead, J.D., 2013. U–Pb detrital zircon analysis — results of an inter-laboratory comparison. Geostand. Geoanal. Res. 37, 243–259.

Kozdon, R., Kita, N.T., Huberty, J.M., Fournelle, J.H., Johnson, C.A., Valley, J.W., 2010. In situ sulfur isotope analysis of sulfide minerals by SIMS: precision and accuracy, with application to thermometry of ~3.5 Ga Pilbara cherts. Chem. Geol. 275, 243–253.

Krogh, T.E., 1973. A low-contamination method for hydrothermal decomposition of zircon and extraction of U and Pb for isotopic age determinations. Geochim. Cosmochim. Acta 37, 485–494.

Krogh, T.E., Corfu, F., Davis, D.W., Dunning, G.R., Heaman, L.M., Kamo, S.L., Machado, N., Greenough, J.D., Nakamura, E., 1987. Precise U–Pb isotopic ages of diabase dykes and mafic to ultramafic rocks using trace amounts of baddeleyite and zircon. In: Halls, H.C., Fahrig, W.F. (Eds.), Mafic Dyke Swarms: Geological Association of Canada Special Paper, 34, pp. 147–152.

Li, Q.-L., Li, X.-H., Liu, Y., Tang, G.-Q., Yang, J.-H., Zhu, W.-G., 2010. Precise U–Pb and Pb–Pb dating of Phanerozoic baddeleyite by SIMS with oxygen flooding technique. J. Anal. At. Spectrom. 25, 1107–1113.

LieWen, Xie, YanBin, Zhang, HuiHuang, Zhang, JingFeng, Sun, FuYuan, Wu, 2008. In situ simultaneous determination of trace elements, U–Pb and Lu–Hf isotopes in zircon and baddeleyite. Chin. Sci. Bull. 53, 1565–1573.

Mattinson, J.M., 1987. U–Pb ages of zircons: a basic examination of error propagation. Chem. Geol. 151–162.

McLean, N.M., Bowring, J.F., Bowring, S.A., Schoene, R.B., 2008. More than just an age: quantitative analysis of geochronological data and uncertainty. Abstr. Programs - Geol. Soc. Am. 40 (6), 134.

McSween Jr., H.Y., 1981. Petrology of the Ogden gabbroic intrusion, York County, South Carolina. S. C. Geol. 25, 91–100.

McSween, H.Y., Sando, T.W., Clark, S.R., Harden, J.T., Strange, E.A., 1984. The gabbro-metagabbro association of the southern Appalachian Piedmont. Am. J. Sci. 284, 437–461.

Mezger, K., Krogstad, E.J., 1997. Interpretation of discordant U-Pb zircon ages: An evaluation. J. metamorphic Geol. 15, 127–140.

Moser, D.E., Chamberlain, K.R., Tait, K.T., Schmitt, A.K., Darling, J.R., Barker, I.R., Hyde, B.C., 2013. Solving the Martian meteorite age conundrum using micro-baddeleyite and launch-generated zircon. Nature 499, 454–457.

Murakami, T., Chakoumakos, B.C., Ewing, R.C., Lumpkin, G.R., Weber, W.J., 1991. Alpha-Decay Event Damage in Zircon. American Mineralogist, United States, p. 76.
Nance, R.D., Gutiérrez-Alonso, G., Keppie, J.D., Linnemann, U., Murphy, J.B., Quesada, C., Strachan, R.A., Woodcock, N.H., 2010. Evolution of the Rheic Ocean. Gondwana Res. 17, 194–222.
Niihara, T., 2011. Uranium–lead age of baddeleyite in shergottite Roberts Massif 04261: implications for magmatic activity on Mars. J. Geophys. Res. 116, E12008.
Paces, J.B., Miller Jr., J.D., 1993. Precise U–Pb ages of Duluth Complex and related mafic intrusions, northeastern Minnesota: geochronological insights to physical, petrogenetic, paleomagnetic, and tectonomagmatic processes associated with the 1.1 Ga midcontinent rift system. J. Geophys. Res. 98 (13997-14-013).
Patchett, P.J., Tatsumoto, M., 1980. A routine high-precision method for Lu–Hf isotope geochemistry and chronology. Contrib. Mineral. Petrol. 75, 263–267.
Patchett, P., Kouvo, O., Hedge, C., Tatsumoto, M., 1981. Evolution of continental-crust and mantle heterogeneity — evidence from Hf isotopes. Contrib. Mineral. Petrol. 78, 279–297.
Paton, C., Woodhead, J.D., Hellstrom, J.C., Hergt, J.M., Greig, A., Maas, R., 2010. Improved laser ablation U–Pb zircon geochronology through robust downhole fractionation correction. Geochem. Geophys. Geosyst. 11, Q0AA06.
Renna, M.R., Tiepolo, M., Tribuzio, R., 2011. In situ U–Pb geochronology of baddeleyite–zircon pairs using laser-ablation ICPMS: the case-study of quartz gabbro from Varney Nunatak (central Victoria Land, Antarctica). Eur. J. Mineral. 23, 223–240.
Rioux, M., Bowring, S., Dudás, F., Hanson, R., 2010. Characterizing the U–Pb systematics of baddeleyite through chemical abrasion: application of multi-step digestion methods to baddeleyite geochronology. Contrib. Mineral. Petrol. 160, 777–801.
Rodionov, N.V., Belyatsky, B.V., Antonov, A.V., Kapitonov, I.N., Sergeev, S.A., 2012. Comparative in-situ U–Th–Pb geochronology and trace element composition of baddeleyite and low-U zircon from carbonatites of the Palaeozoic Kovdor alkaline–ultramafic complex, Kola Peninsula, Russia. Gondwana Res. 21, 728–744.
Russell, W.A., Papanastassiou, D.A., Tombrello, T.A., 2002. Ca isotope fractionation on the Earth and other solar system materials. Geochim. Cosmochim. Acta 42, 1075–1090.
Schärer, U., 1984. The effect of initial ^{230}Th disequilibrium on young U–Pb ages: the Makalu case, Himalaya. Earth Planet. Sci. Lett. 67, 191–204.
Scherer, E.E., Münker, C., Mezger, K., 2001. Calibration of the Lutetium–Hafnium clock. Science 293, 683–687.
Schmitt, A.K., 2007. Ion microprobe analysis of (^{231}Pa)/(^{235}U) and an appraisal of protactinium partitioning in igneous zircon. Am. Mineral. 92, 691–694.
Schmitt, A.K., Chamberlain, K.R., Swapp, S.M., Harrison, T.M., 2010. In situ U–Pb dating of micro-baddeleyite by secondary ion mass spectrometry. Chem. Geol. 269, 386–395.
Scoates, J.S., Chamberlain, K.R., 1995. Baddeleyite (ZrO_2) and zircon ($ZrSiO_4$) from anorthositic rocks of the laramie anorthosite complex, Wyoming: Petrologic consequences and U–Pb ages. Am. Mineral. 80, 1317–1327.
Sickafus, K.E., Matzke, H., Hartmann, T., Yasuda, K., Valdez, J.A., Chodak III, P., Nastasi, M., Verrall, R.A., 1999. Radiation damage effects in zirconia. J. Nucl. Mater. 274, 66–77.
Simeone, D., Gosset, D., Bechade, J.L., Chevarier, A., 2002. Analysis of the monoclinic–tetragonal phase transition of zirconia under irradiation. J. Nucl. Mater. 300, 27–38.
Simeone, D., Baldinozzi, G., Gosset, D., Le Caër, S., 2006. Phase transition of pure zirconia under irradiation: a textbook example. Nucl. Instrum. Methods Phys. Res., Sect. B 250, 95–100.
Söderlund, U., Johansson, L., 2002. A simple way to extract baddeleyite (ZrO_2). Geochem. Geophys. Geosyst. 3, 1014.
Söderlund, U., Patchett, J., Vervoort, J., Isachsen, C., 2004. The Lu-176 decay constant determined by Lu–Hf and U–Pb isotope systematics of Precambrian mafic intrusions. Earth Planet. Sci. Lett. 219, 311–324.
Söderlund, U., Isachsen, C., Bylund, G., Heaman, L., Jonathan Patchett, P., Vervoort, J., Andersson, U., 2005. U–Pb baddeleyite ages and Hf, Nd isotope chemistry constraining repeated mafic magmatism in the Fennoscandian Shield from 1.6 to 0.9 Ga. Contrib. Mineral. Petrol. 150, 174–194.
Söderlund, U., Elming, S.-A., Ernst, R.E., Schissel, D., 2006. The central Scandinavian dolerite group — protracted hotspot activity or back-arc magmatism? Constraints from U–Pb baddeleyite geochronology and Hf isotopic data. Precambrian Res. 150, 136–152.
Söderlund, U., Hellström, F.A., Kamo, S.L., 2008. Geochronology of high-pressure mafic granulite dykes in SW Sweden: tracking the P–T–t path of metamorphism using Hf isotopes in zircon and baddeleyite. J. Metamorph. Geol. 26, 539–560.
Söderlund, U., Ibanez-Mejia, M., Bahat, A., Ernst, R.E., Ikenne, M., Soulaimani, A., Youbi, N., Cousens, B., Janati, M., Hafid, A., 2013. Reply to comment on "U–Pb baddeleyite ages and geochemistry of dolerite dykes in the Bas-Drâa inlier of the anti-atlas of Morocco: newly identified 1380 Ma event in the West African Craton" by André Michard and Dominique Gasquet. Lithos 1–8.
Stacey, J., Kramers, J., 1975. Approximation of terrestrial lead isotope evolution by a two-stage model. Earth Planet. Sci. Lett. 26, 207–221.
Suominen, V., 1991. The chronostratigraphy of southwestern Finland with special reference to Postjotnian and Subjotnian diabases. Geol. Surv. Finland Bull. 356, 106.
Sylvester, P., Ghaderi, M., 1997. Trace element analysis of scheelite by excimer laser-ablation-inductively coupled plasma-mass spectrometry (ELA-ICP-MS) using a synthetic silicate glass standard. Chem. Geol. 141, 49–65.
Taylor, R., Clark, C., Reddy, S.M., 2012. The effect of grain orientation on secondary ion mass spectrometry (SIMS) analysis of rutile. Chem. Geol. 300, 81–87.
Thirlwall, M.F., Walder, A.J., 1995. In situ hafnium isotope ratio analysis of zircon by inductively coupled plasma multiple collector mass spectrometry. Chem. Geol. 122, 241–247.
Thomson, S.N., Gehrels, G.E., Ruiz, J., Buchwaldt, R., 2012. Routine low-damage apatite U–Pb dating using laser ablation-multicollector-ICPMS. Geochem. Geophys. Geosyst. 13, Q0AA21.
Valdez, J.A., Chi, Z., Sickafus, K.E., 2008. Light ion irradiation-induced phase transformation in the monoclinic polymorph of zirconia. J. Nucl. Mater. 381, 259–266.
Valley, J., Kita, N., 2009. In-situ oxygen isotope geochemistry by ion microprobe. Mineralogical Association of Canada Short Course, 41, pp. 19–63.
van Staal, C.R., 2007. Pre-Carboniferous tectonic evolution and metallogeny of the Canadian Appalachians. In: Goodfellow, W.D. (Ed.), Mineral Resources of Canada: A Synthesis of Major Deposit Types, District Metallogeny, the Evolution of Geological Provinces, and Exploration Methods. Mineral Deposit Division of the Geological Association of Canada and the Geological Survey of Canada, pp. 793–818.
Vervoort, J., Blichert-Toft, J., 1999. Evolution of the depleted mantle: Hf isotope evidence from juvenile rocks through time. Geochim. Cosmochim. Acta 63 (3), 533–556.
Vervoort, J., Patchett, P., Soderlund, U., Baker, M., 2004. Isotopic composition of Yb and the determination of Lu concentrations and Lu/Hf ratios by isotope dilution using MC-ICPMS. Geochem. Geophys. Geosyst. 5, Q11002.
Wingate, M., Compston, W., 2000. Crystal orientation effects during ion microprobe U–Pb analysis of baddeleyite. Chem. Geol. 168, 75–97.
Woodhead, J.D., Hergt, J.M., 2005. A preliminary appraisal of seven natural zircon reference materials for in situ Hf isotope determination. Geostand. Geoanal. Res. 29, 183–195.
Woodhead, J., Hergt, J., Shelley, M., Eggins, S., Kemp, R., 2004. Zircon Hf-isotope analysis with an excimer laser, depth profiling, ablation of complex geometries, and concomitant age estimation. Chem. Geol. 209, 121–135.
Wu, F.-Y., Yang, Y.-H., Xie, L.-W., Yang, J.-H., Xu, P., 2006. Hf isotopic compositions of the standard zircons and baddeleyites used in U–Pb geochronology. Chem. Geol. 234, 105–126.
Wu, F.-Y., Yang, Y.-H., Mitchell, R.H., Bellatreccia, F., Li, Q.-L., Zhao, Z.-F., 2010. In situ U–Pb and Nd–Hf–(Sr) isotopic investigations of zirconolite and calzirtite. Chem. Geol. 277, 178–195.
Wu, F.-Y., Yang, Y.-H., Li, Q.-L., Mitchell, R.H., Dawson, J.B., Brandl, G., Yuhara, M., 2011. In situ determination of U–Pb ages and Sr–Nd–Hf isotopic constraints on the petrogenesis of the Phalaborwa carbonatite Complex, South Africa. Lithos 127, 309–322.
Yuan, H., Gao, S., Liu, X., Li, H., Günther, D., FuYuan, Wu., 2004. Accurate U–Pb age and trace element determinations of zircon by laser ablation-inductively coupled plasma-mass spectrometry. Geostand. Geoanal. Res. 28, 353–370.